Structure of Space-time Correlations of Bursting Phenomenon in an Open-channel Flow

By

Hiroji NAKAGAWA*, Iehisa NEZU*
and Naoya MATSUMOTO**

(Received September 29, 1979)

Abstract

The present study is to investigate the structure of space-time correlations of bursting motions, such as ejections and sweeps in an open-channel flow, by a new conditional sampling method in which simultaneous measurements of the instantaneous Reynolds stress have been performed by two dual-hot-film probes. One probe was fixed near the edge of buffer layer and used as a detecting probe of the bursting motions, while the other probe was moved in both the streamwise and flow-depth-wise directions. The main conclusions obtained from the above are as follows:

(1) The spatial and time scales of the streamwise turbulent velocity component are larger than those of the vertical velocity component.

(2) The spatial and time scales of the sweep motion are also larger than those of the ejection motion.

(3) The spatial scale of the ejection motion extends more widely downstream than upstream, and vice versa for the sweep motion.

(4) The bursting motion is a kind of a large-scale eddy structure, and its coherent structure is fairly inclined downstream toward the wall. It is convected downstream with a longer life-time than the bursting passing-period, namely in the frozen-turbulence-like manner.

Next, a qualitative model is proposed which attempts to explain the space-time structures of the bursting phenomenon, on the basis of the above anemometry information and other visual information.

1. Introduction

In the past ten years intensive experimental research on the turbulence-production mechanism and the bursting phenomenon over a smooth solid bed has been performed by making use of various visual methods and conditional point-measurements by hot-wire or hot-film anemometers. As the result of this research, the

---

* Department of Civil Engineering.
** Ministry of Construction.

physics of solid-wall turbulence has now been fairly established, at least in a qualitative sense. For example, Hinze (1975)[1] and Willmarth(1975)[2] have written excellent reviews which describe the recent status of research on solid-wall turbulence, especially on the bursting phenomenon of turbulent boundary layers. Also, they have pointed out the necessity of research on the structure of the instantaneous Reynolds stress in order to make clear the bursting phenomonon near the wall. The authors (1977)[3] have investigated in detail the contributions to the Reynolds stress from bursting events in open-channel flows by conditionally analyzing the instantaneous Reynolds-stress fluctuations obtained from the hot-film anemometers.

Next, the authors (1978)[4] have proposed a new evaluation method for the bursting period, on the basis of the phenomenological consideration that the number of the occurrences of interaction-like motions should be removed from those of the ejection and sweep events in the sorted Reynolds-stress fluctuating signals. Then, they have examined the periodic characteristics of the bursting phenomenon in the Eulerian observation, by systematically varying the Reynolds and Froude numbers as well as the wall roughness. Furthermore, the authors (1979)[5] have recently extended these conditional sampling methods of the instantaneous Reynolds stress, and investigated the effect of suction or injection on the mechanism of turbulence-production in a permeable open-channel flow.

Several theoretical models by which the mechanism of wall turbulence and the bursting process can be explained even quantitatively have been proposed, on the basis of much experimental knowledge of the bursting phenomenon. These models may be roughly classified into two groups. One is a renewal model which was originally proposed by Einstein & Li (1956)[6], and the other is a waveguide model which was originally proposed by Landahl (1967)[7]. Black(1968)[8] developed a renewal model in which the formation and breakdown of the horseshoe vortex was considered in a repetitive way. He could successfully explain several turbulence characteristics even quantitatively, although the governing equation was a one-dimensional and linear equation, similar to the Einstein-Li model. Recently, the authors(1978)[4] also proposed a modified renewal model which was inherently quasi-two-dimensional and quasi-linear in regard to the streamwise and normal velocities u and v, on the basis of the Einstein-Li model and also the knowledge of the bursting-period characteristics. They could satisfactorily explain fairly well, even quantitatively, a sequence of the bursting process near the wall, as well as the distributions of mean velocity, turbulence intensities, Reynolds stress etc.

On the other hand, a waveguide model was developed by Bark (1975)[9] and Landahl (1977)[10]. They considered the wave-type motions with Fourier components and derived a linear non-homogeneous Orr-Sommerfeld equation in which the non-

linear terms of Reynolds stress were regarded as a known forcing function. Then, by assuming that these non-linear forcing terms, i. e. the instantaneous Reynolds stresses, were a random distribution of delta functions in the streamwise and spanwise directions x, z and the time t with a variation with the normal direction y inferred from the experimental data, they could theoretically obtain the spectral distributions of fluctuating velocities, which were in good agreement with the experimental values.

Although the waveguide model seems to be more sophisticated than the renewal model, the former probably cannot explain the bursting mechanism better than the latter, because the bursting process itself is considered as a known driving force of the turbulent flow.

It should be noticed that both the renewal and waveguide models are applicable only very near the wall, i. e. $y^+ \leq 50$, since their models are inherently approximated by linear differential equations. However, a closer interrelation between the inner and outer layers, i. e. between the bursting and bulge motions in the boundary layer, has been suggested through visual observation or the hot-wire measurements by Laufer & Narayanan (1971)[11], Blackwelder & Kovasznay (1972)[12], Offen & Kline (1975)[13] and recently by Praturi & Brodkey (1978)[14]. A closer interrelation between the wall and free-surface regions, i. e. the bursting and boiling phenomena in open channel, has been also suggested by Jackson (1976)[15] and the authors (1978)[4].

Therefore, an investigation of the space-time structure of the bursting phenomenon, which occurs originally near the buffer layer and then shows a coherent or organized flow structure during its convection process, will be contributive not only to the confirmation of these suggestions, but also to the refinement of the physical description of the bursting phenomenon.

In the light of the above, the present study is to investigate the structure of space-time correlations of bursting events, such as ejections and sweeps in an open-channel flow, by the conditional sampling of the instantaneous Reynolds-stress signals measured simultaneously at two different points. One probe is fixed near the edge of the buffer layer and used as a detecting probe of the bursting motions, and the other probe is moved in both the streamwise and flow-depth-wise (or normal) directions. The time scales and spatial scales of the ejection and sweep motions occurring originally near the buffer layer, and also their convective characteristics will be considered experimentally. A qualitative model will be then proposed which attempts to explain the space-time structure of the bursting phenomenon in an open-channel flow.

2. Analytic technique

2. 1 Conventional space-time correlations

We consider a fully developed, two-dimensional and normal open-channel flow
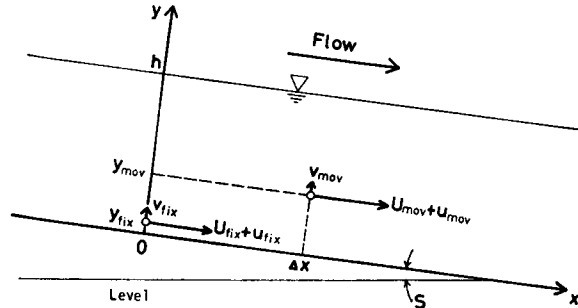
Fig. 1. Open-channel flow field.

field, as shown in Fig. 1. The x coordinate is aligned with the main-stream velocity or the free-surface velocity U_{max}. y is the coordinate perpendicular to the wall, and z is in the spanwise direction. The velocity fluctuations in the x, y and z directions are u, v and w, and also their r. m. s. values, i. e. the turbulence intensities are u', v' and w', respectively.

Since the velocity field is homogeneous in the streamwise (x-axis) and spanwise (z-axis) directions and is also steady in time, the conventional space-time correlations of the velocity components $u_i(x_0, y_0, z_0, t_0)$ and $u_j(x_1, y_1, z_1, t_1)$ are defined by

$$Cu_iu_j(\varDelta x, y_0, y_1, \varDelta z, \tau) = \frac{\overline{u_i(x_0, y_0, z_0, t_0) \cdot u_j(x_1, y_1, z_1, t_1)}}{u_i'(x_0, y_0, z_0) \cdot u_j'(x_1, y_1, z_1)}$$
$$\equiv \overline{\hat{u}_i(x_0, y_0, z_0, t_0) \cdot \hat{u}_j(x_0+\varDelta x, y_1, z_0+\varDelta z, t_0+\tau)} \qquad (1)$$

where, suffix i and j are 1, 2 or 3, i. e. $u_1=u$, $u_2=v$ and $u_3=w$. $\hat{u}_i$ is the velocity fluctuation normalized by its turbulence intensity u_i', that is, $\hat{u}_i \equiv u_i/u_i'$. $\varDelta x \equiv (x_1-x_0)$, (y_1-y_0) and $\varDelta z \equiv (z_1-z_0)$ are the spatial separations, and $\tau \equiv (t_1-t_0)$ is the time lag. The signal $u_i(x_0, y_0, z_0, t_0)$ from the fixed probe was recorded and shifted in time. It was then correlated with the signal $u_j(x_1, y_1, z_1, t_1)$ from the movable probe which was located upstream or downstream. Of course, by denoting that $i=1$, $j=2$, $y_0=y_1=y$ and $\varDelta x=\varDelta z=\tau=0$, we can obtain the correlation coefficient of the Reynolds stress $-\overline{uv}$, as follows:

$$R(y) \equiv \frac{-\overline{uv}}{u'v'} = -Cuv(0, \ y, \ y, \ 0, \ 0) = -\overline{\hat{u}(y, \ t) \cdot \hat{v}(y, \ t)} \qquad (2)$$

2. 2   A new conditional analysis of space-time correlations

Although the bursting phenomenon occurs fairly random at one place or time, a sequence of its bursting events has a quasi-ordered process. It seems, therefore, that its significant information cannot be obtained by the conventional 'long-time' averaging

technique such as Eq. (1), as has been pointed out by many researchers[2],[3],[4],[16]. Hence, a conditional sampling method which detects the significant information from the fluctuating velocity signals has been explored by Kovasznay et al. (1970)[17]. In general, the conditional average of an arbitrary signal $q(x, y, z, t+\tau)$ can be defined as follows:

$$<q>(x_1, y_1, z_1, \tau) = \frac{\int_T q(x_1, y_1, z_1, t+\tau) \cdot I(x_0, y_0, z_0, t)dt}{\int_T I(x_0, y_0, z_0, t)dt} \qquad (3)$$

where, $\int_T \cdots\cdots dt$ means $\lim\limits_{T\to\infty} T^{-1} \int_0^T \cdots\cdots dt$. $I(x_0, y_0, z_0, t)$ is the detecting function of the turbulence phenomenon in question which occurs at the point of (x_0, y_0, z_0, t). For example, the detecting function $I(x_0, y_0, z_0, t)$ of the bulges phenomenon in the boundary layer can be definitely given by the intermittency function, as follows[17]:

$$I(x_0, y_0, z_0, t) = \begin{cases} 1 & \text{for turbulent flow} \\ 0 & \text{for non-turbulent flow} \end{cases} \qquad (4)$$

However, the detecting function $I(t)$ of the bursting phenomenon near the wall is not yet sufficiently established at present, although several detecting functions have been proposed by Lu & Willmarth (1973)[18], Brodkey et al. (1974)[19], Blackwelder & Kaplan (1976)[20], Wallace et al. (1977)[21], Nakagawa & Nezu (1978)[4] and others. As already pointed out in our previous paper (1978)[4], the instantaneous Reynolds-stress signals $u(t)v(t)$ can be reasonably used as discriminating information, since they are directly related to the bursting phenomenon or the mechanism of turbulence-production. Then, the sorting functions of ejection, $I_e(t)$, sweep, $I_s(t)$, outward-interaction, $I_o(t)$, and inward-interaction, $I_i(t)$, are defined, respectively, as follows:

$$I_e(t) \equiv I_2(t) = \begin{cases} 1 & \text{for } u(t)<0 \text{ and } v(t)>0 \\ 0 & \text{otherwise} \end{cases} \qquad (5)$$

$$I_s(t) \equiv I_4(t) = \begin{cases} 1 & \text{for } u(t)>0 \text{ and } v(t)<0 \\ 0 & \text{otherwise} \end{cases} \qquad (6)$$

$$I_o(t) \equiv I_1(t) = \begin{cases} 1 & \text{for } u(t)>0 \text{ and } v(t)>0 \\ 0 & \text{otherwise} \end{cases} \qquad (7)$$

$$I_i(t) \equiv I_3(t) = \begin{cases} 1 & \text{for } u(t)<0 \text{ and } v(t)<0 \\ 0 & \text{otherwise} \end{cases} \qquad (8)$$

Here, the ejection and sweep events are mainly considered, because these events contribute mostly to the Reynolds stress or the turbulence production[3].

Unfortunately, $I_e(t)$ or $I_s(t)$ should not be regarded directly as a detecting function $I(t)$ for the bursting motions, because the ejection and sweep events in the sorted Reynolds-stress signals still contain the interaction-like motions, as has been pointed out

by the authors[4]. So, Lu & Willmarth[18], as well as the authors[4][5], introduced a threshold level H in the Reynolds-stress signals, and assumed that the bursting motions occur only when $|u(t)v(t)| \geq H$. However, the determination of the threshold level H is more or less arbitrary. Therefore, we adopt a new detecting function weighted by the instantaneous Reynolds-stress signal itself, i. e. $I(t) \equiv u(t)v(t) \cdot I_e(t)$, etc. Then, the conditional average of the space-time correlations of ejection and sweep motions can be definitely given by, respectively,

$$\langle q \rangle_e(x_1, y_1, z_1, \tau) = \frac{\int_T q(x_1, y_1, z_1, t+\tau) \cdot \{u(t)v(t)I_e(t)\}_0 dt}{\int_T \{u(t)v(t)I_e(t)\}_0 dt} \tag{9}$$

$$\langle q \rangle_s(x_1, y_1, z_1, \tau) = \frac{\int_T q(x_1, y_1, z_1, t+\tau) \cdot \{u(t)v(t)I_s(t)\}_0 dt}{\int_T \{u(t)v(t)I_s(t)\}_0 dt} \tag{10}$$

where, the suffix $\{\ \}_0$ denotes the position of the detecting probe. (9) or (10) means that the stronger the instantaneous Reynolds-stress is, the larger contribution is given in the average structure of the bursting phenomenon.

Such a weighted detecting function seems to be more useful and reasonable than a detecting function with a threshold level H. This is because a more objective evaluation can be carried out without arbitrary parameters. Also, the random values such as the background turbulence are apt to be canceled by each other because of the larger numbers of data averaged than in the case of $|u(t)v(t)| \geq H$. The obvious validity of (9) and (10) will be shown through the following experimental considerations.

3. Experimental equipment and procedures

The experiments on a two-dimensional, fully developed and normal turbulent flow in a smooth open-channel, whose hydraulic conditions are described in Table 1, were

Table 1. Hydraulic parameters for the experiment.

Bed slope	S	8.0×10^{-5}
Channel width	B	50cm
Flow depth	h	8.1 cm
Aspect ratio	B/h	6.2
Discharge	Q	6.0 l/sec
Free-surface velocity	U_{max}	21.2 cm/sec
Mean velocity	U_m	14.9 cm/sec
Friction velocity	U_*	0.95 cm/sec
Water temperature	T_w	20.7°C
Reynolds number	$R_e = U_m h/\nu$	1.2×10^4
	$R_* = U_* h/\nu$	774
Froude number	$F_r = U_m/\sqrt{gh}$	0.17

(a) Configuration of hot-films
  ($\Delta x > 0$, Side view)

Flow

Moved Probe

Fixed Probe

(b) Configuration of hot-films
  ($\Delta x < 0$, Side view)

Flow

Moved Probe

Fixed Probe

(c) Configuration of hot-films
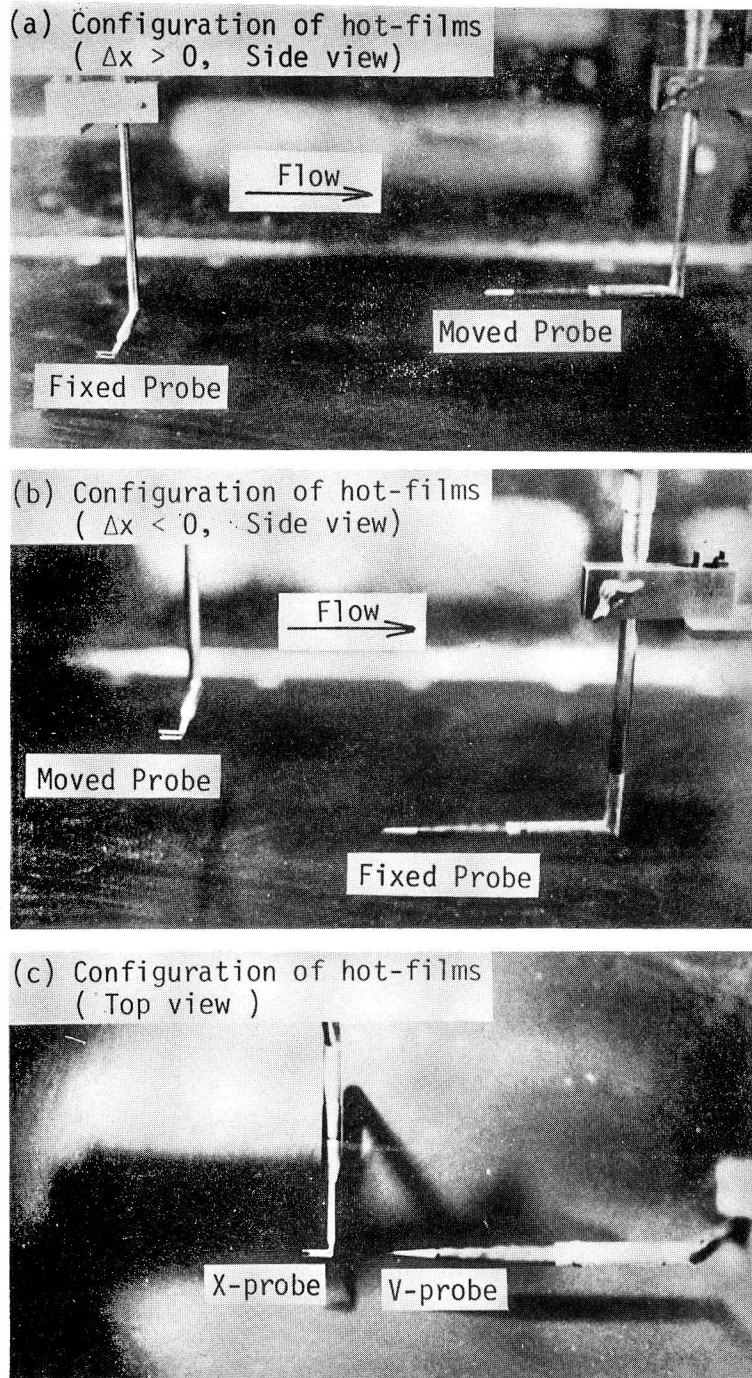 (Top view)

X-probe   V-probe

Photo 1. Configuration of two hot-film probes.

conducted in a tilting flume 15m long, 50cm wide and 30cm deep. This experimental set-up was the same as that previously used by the authors[3],[4],[5]. The flow depth h was 8cm and the mean velocity U_m was 15cm/sec. As for results, the Reynolds number was $R_e \equiv U_m h/\nu = 1.2 \times 10^4$ or $R_* \equiv U_* h/\nu = 774$ (where, U_* is the friction velocity). The Froude number was $F_r \equiv U_m/\sqrt{gh} = 0.17$, whose hydraulic conditions were nearly the same as those in our previous studies[3],[4],[5].

Only the correlations between (u_0, v_0) and (u_1, v_1) at a couple of points in the $x-y$ plane (see Fig. 1) were measured by using two sets of dual-sensor hot-film anemometers, i.e. an X-type probe (DISA 55R64) and a V-type probe (DISA 55A89). A reasonable configuration of these hot-film probes was prepared in order to avoid any interference from the wake of the upstream probe. As shown in Photo 1, the X-type fiber-film probe with two pairs of needles of 9.1mm length was adopted as the upstream probe. The V-type wedge-film probe with 100mm straight length in the streamwise direction was used as the downstream probe. The rod of the upstream probe with 2.3mm diameter and 65mm length was laid in the $x-z$ plane and perpendicular to the x-axis (see Photo 1 (c)). Two probes were spaced about 2mm in the spanwise direction when Δx was comparatively small so as to move the probe easily. Thus, the small wakes behind the needles of the upstream probe will hardly influence the downstream probe. However, it was suggested that this separation distance of Δz was so large that $C_{uu}(\Delta x, y_0, y_1, \Delta z, \tau)$ cannot be regarded even approximately as $C_{uu}(\Delta x, y_0, y_1, 0, \tau)$ when Δx was small.

The detecting probe was fixed at $y_0 = 4$mm ($y_0/h = 0.05$, $y_0^+ \equiv y_0 U_*/\nu = 38$), since the bursting phenomenon occurs most violently below or near this position[2],[3]. The movable probe was set at the different 222 points in number in the $x-y$ plane, as shown in Fig. 2. That is, $y_1 = 0.4, 0.7, 1.3, 2.4, 4.0$ and 6.0cm, which were the representative points in the wall region ($y^+ \leq 100$), the equilibrium region ($100 \leq y^+$ and $y/h \leq 0.6$) and the free-surface region ($y/h \geq 0.6$) (see Nezu (1977 a)[22]). From the fact that the streamwise spatial scale λ_1 of the bursting phenomenon was the order of $4h$ (see Hinze (1975)[1] and Nakagawa & Nezu (1978)[4]), $|\Delta x|$ was varied up to $4h$ so as to be smaller in the neighbourhood of the fixed probe. By these point-measurements, the structure of space-time correlations of bursting phenomenon occurring near the wall was expected to be clarified fairly well.

The output signals of the anemometers were recorded in analog form by using an FM tape recorder for about two minutes at each measured point. The effects of impurities or bubbles in the water were almost negligible in this duration and thus a most stable operation was obtained. The output signals were then reproduced for converting into digital form, with the sample size $N = 10000$ and the sampling frequency $f = 100$ Hz, that is, the average-evaluation time $T = N/f = 100$ seconds.
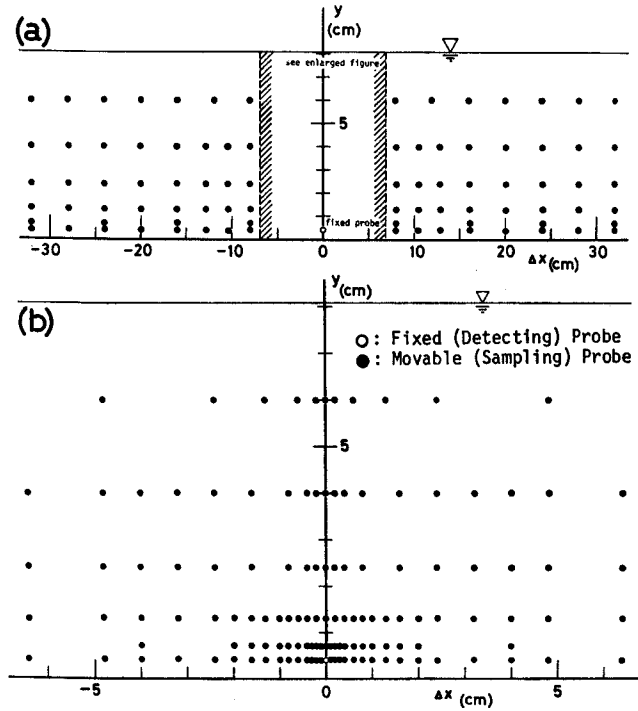
Fig. 2. Coordinates of the measurement points of the movable probe.

Next, the hot-film anemometers were calibrated by towing the probe over a fixed length (about 200cm) in still water, by making use of a movable carriage driven by a variable motor before and after the experiments. Consequently, the output voltage signals could be easily converted into the velocity signals through these calibration curves. Then, some statistical analyses described previously were carried out by a large digital computer, the FACOM M-190, at the Data Processing Center, Kyoto University. Most of the results were then plotted by an on-line X-Y plotter.

4. Experimental results and discussion

4. 1 Examination of some basic quantities of turbulence

Since the mean velocity distribution U measured by both the X-type and V-type probes satisfied the log-law very well, the friction velocity U_* was firstly evaluated from this logarithmic distribution. Next, the experimental values of the Reynolds stress $-\overline{uv}/U_*^2$ were examined. These values showed a good agreement with the theoretical curve which is described by[22]

$$-\frac{\overline{uv}}{U_*^2} = (1-y/h) - \frac{2(1-y^+/R_*)}{1+\sqrt{1+4\,l^{+2}(1-y^+/R_*)}}$$

(11)
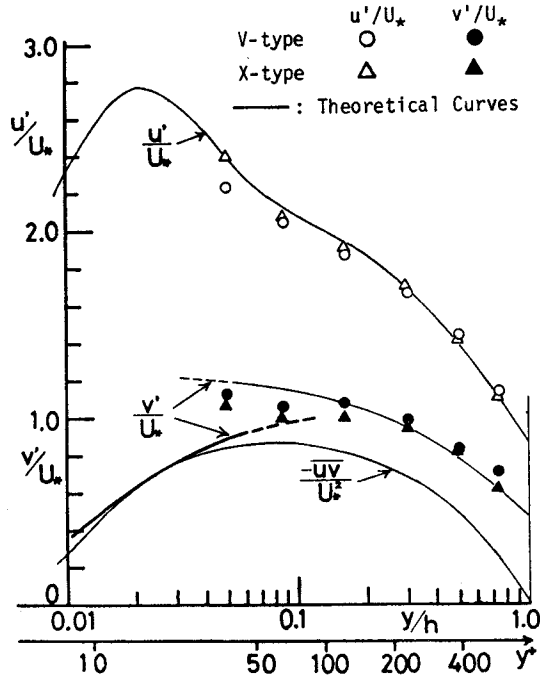
Fig. 3. Distributions of turbulence intensities and Reynolds stress.

where, l^+ is the dimension-less mixing-length, which is given by the van Driest-type. It is more desirable, however, to correct the calibration coefficients of each hot–film sensor which were separately determined by the calibration, so that the output data of $-\overline{uv}$ obtained from the cross operation of each sensor signal may coincide perfectly with the theoretical values of (11), as shown in Fig. 3. This is because the output signals of $u(t) \cdot v(t)$ are essential quantities for investigating the bursting phenomenon, as mentioned previously. In the present experiment, this correction was within only 5%.

Fig. 3 shows the experimental values of the turbulence intensities u'/U_* and v'/U_*, which are ensemble-averaged among the data obtained at all streamwise positions x_1 for each height y_1. The authors have derived the theoretical curves of the turbulence intensities in the renewal model[4], the Π-eddy model[23],[28] and the combined model[22], as follows:

$$\frac{u'}{U_*} = (1 - \exp(-y^+/A)) \cdot D_1 \exp(-y^+/R_*) + \exp(-y^+/A) \cdot By^+ \qquad (12)$$

$$\frac{v'}{U_*} = \begin{cases} \text{implicit description by the renewal model for } y^+ < 50 \\ D_2 \exp(-y^+/R_*) \quad \text{for } y^+ \geq 50 \end{cases} \qquad (13)$$
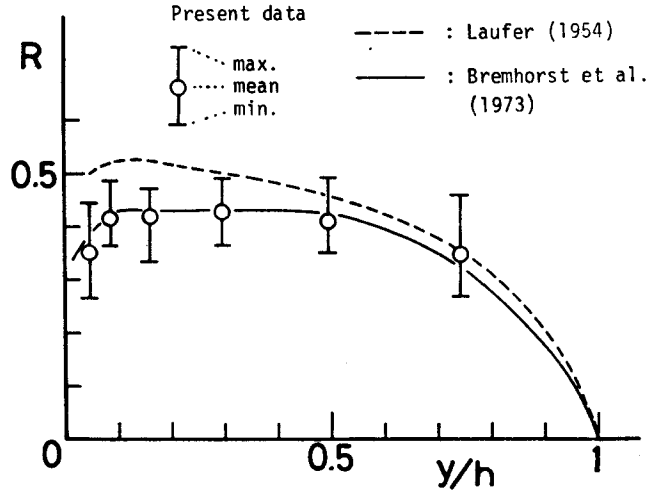
Fig. 4. Correlation coefficient of the Reynolds stress.

where, $A=10$, $B=0.3$, $D_1=2.3$ and $D_2=1.27$.

The experimental values of u'/U_* and v'/U_* measured by both the X-type and V-type probes are in good agreement with (12) and (13), as well as the data obtained previously[4],[5],[23].

Fig. 4 shows the correlation coefficient $R(y)$ of the Reynolds stress which is given by (2). The scatter among these data at the different position x_1 is shown by the maximum, mean and minimum values. Their mean values agree well with the experimental values given by many researchers[22]. Also, the scatter of the present data is almost within that of the previous data.

Furthermore, in order to examine the interference of the wake of the upstream probe, the contribution rates RS_j of each bursting event to the Reynolds stress are shown in Fig. 5, as a function of $\Delta x/h$ for $y_0/h=y_1/h=0.05$. They are the essential characteristic values, on analyzing the bursting phenomenon, and are defined as follows:[3]

$$RS_j = \overline{u(t)v(t) \cdot I_j(t)} / \overline{u(t)v(t)} \quad (j=1,2,3 \text{ and } 4) \tag{14}$$

where, $j=1$ (outward-interaction), $j=2$ (ejection), $j=3$ (inward-interaction) and $j=4$ (sweep). So, $I_j(t)$ is given by (5)$\sim$(8).

The mean value and its standard deviation of RS_j are also described in Fig. 5, respectively. Variation of the measured data of RS_j does not show any systematic trend against $\Delta x/h$ even when Δx is small. Also, their values of RS_j agree well with previous experimental or theoretical values[3].

From the above examinations, it may be concluded that the present turbulence-
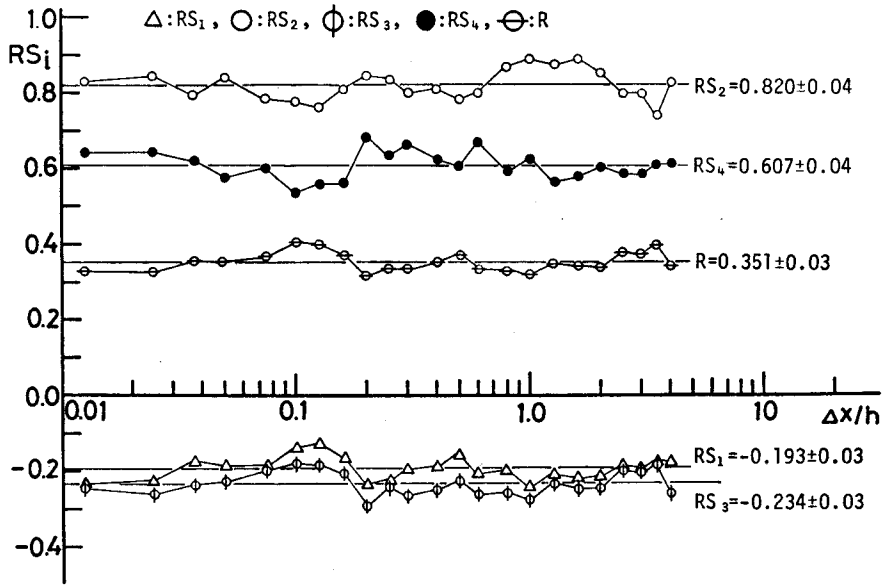
Fig. 5. Contribution rates of each bursting event to the Reynolds stress obtained
at $y^+ = 38$.

measurements by both the X-type and V-type probes are fairly accurate in at least one-point measurement, and that the interference of the wake of the upstream probe is almost negligible.

4. 2 Conventional space-time correlations

Fig. 6 shows some typical examples of the conventional space-time correlations $C_{uu}(\varDelta x, y_{fix}, y_{mov}, \tau)$ and $C_{vv}(\varDelta x, y_{fix}, y_{mov}, \tau)$ which were plotted by the X-Y plotter, where, DX and T_L denote $\varDelta x$ and τ, respectively. In Fig. 7, $C_{uu}(\varDelta x, \tau)$ at $y_0/h = y_1/h = 0.05$ is described in a three-dimensional picture. From these figures, the spatial
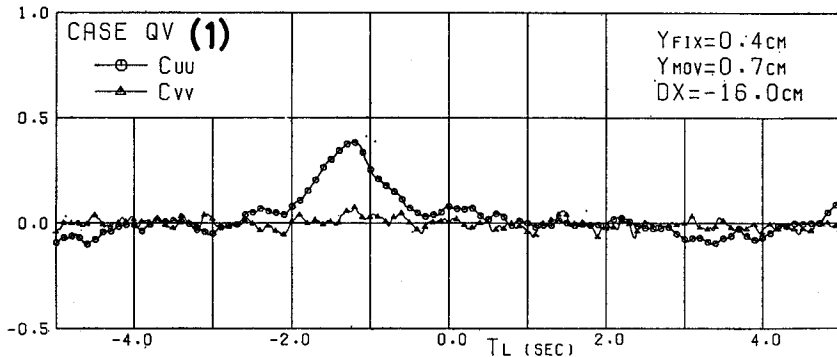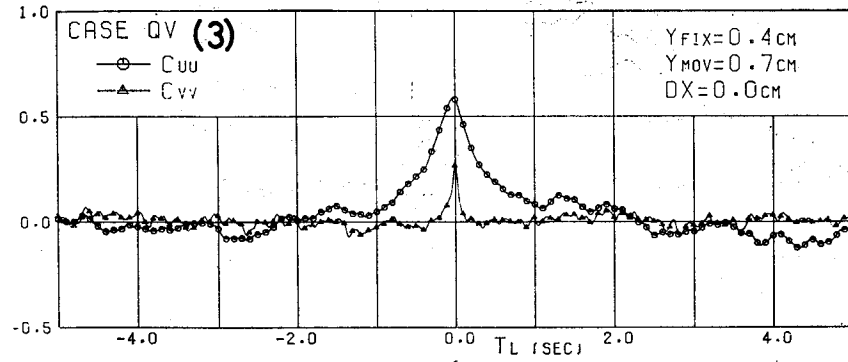

Fig. 6. Conventional long-time averaging space-time correlations of u and v, C_{uu} and C_{vv}.

CASE QV (2)
—⊕— Cuu
—▲— Cvv

YFIX=0.4CM
YMOV=0.7CM
DX=-4.0CM

TL (SEC)

CASE QV (3)
—⊕— Cuu
—▲— Cvv

YFIX=0.4CM
YMOV=0.7CM
DX=0.0CM

TL (SEC)

CASE QV (4)
—⊕— Cuu
—▲— Cvv

YFIX=0.4CM
YMOV=0.7CM
DX=4.0CM

TL (SEC)

CASE QV (5)
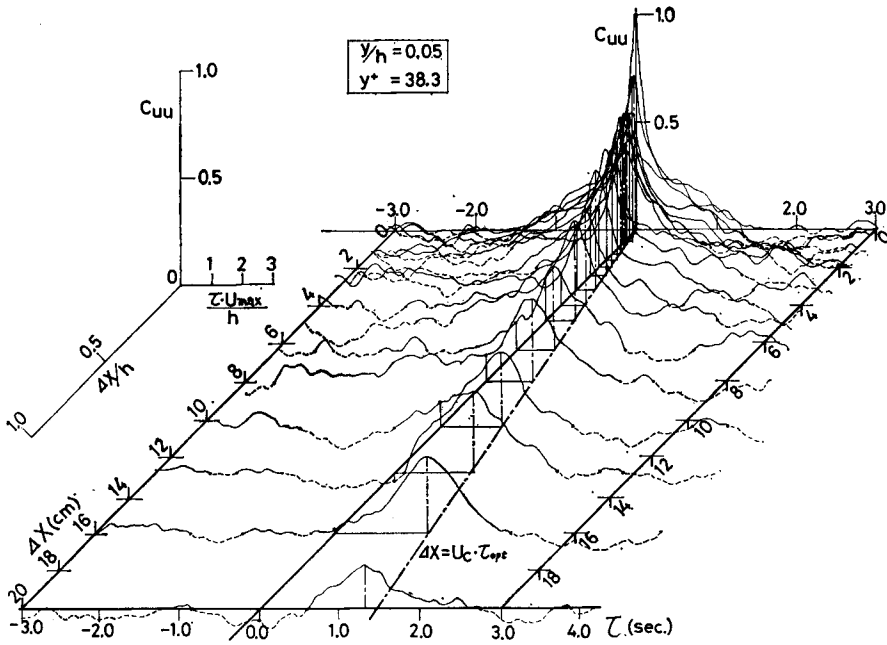—⊕— Cuu
—▲— Cvv

YFIX=0.4CM
YMOV=0.7CM
DX=16.0CM

TL (SEC)
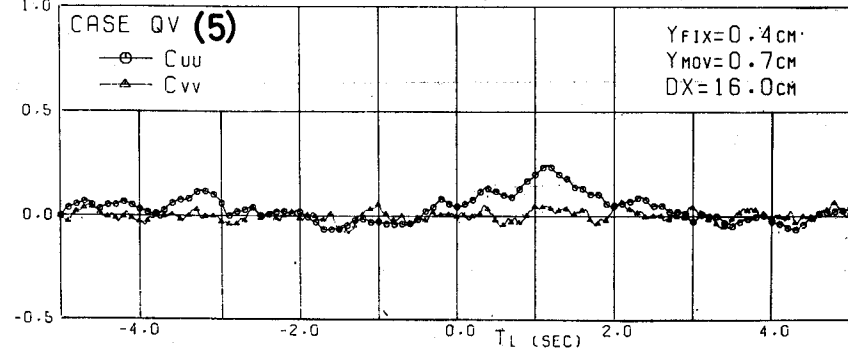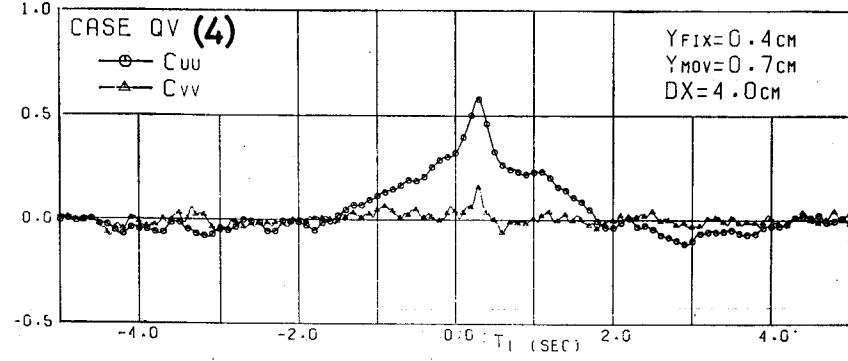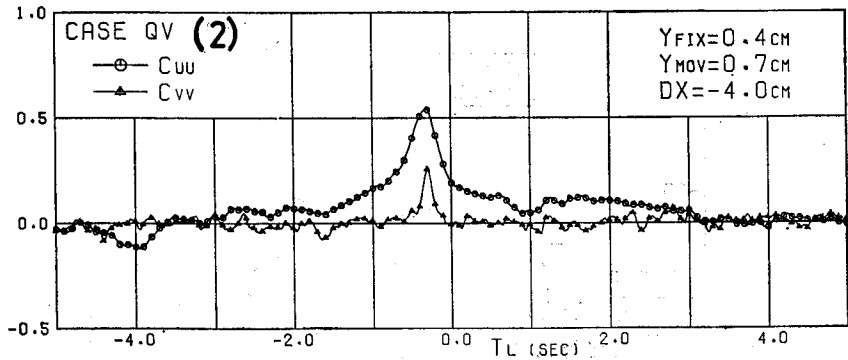
Fig. 7. Longitudinal space-time correlation of C_{uu} obtained at $y^+ = 38$.

scales and the convection process of the u or v velocity component can be obtained in terms of long-time averaging structure, and they are also compared with many previous results[12],[24].

Firstly, the correlation of the v component decays faster in both space and time than does that of the u component. Fig. 8 shows the space correlations $C_{uu}(\varDelta x, \tau = 0)$
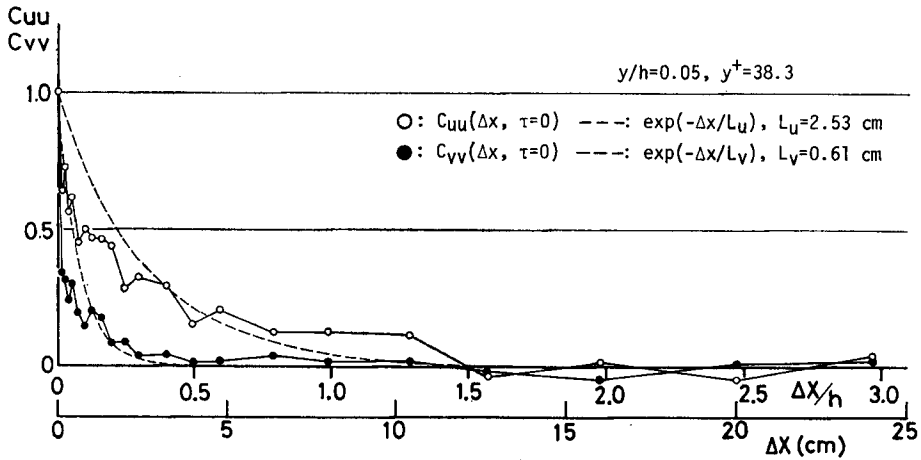

Fig. 8. Space correlations of C_{uu} and C_{vv}.

and $C_{vv}(\Delta x, \tau=0)$ at $y_0/h=y_1/h=0.05$. The mean eddy scale or integral-scale L_u and L_v of u and v are defined, respectively, as follows:

$$L_u = \int_0^{x_{ou}} C_{uu}(\Delta x) d(\Delta x) \tag{15}$$

$$L_v = \int_0^{x_{ov}} C_{vv}(\Delta x) d(\Delta x) \tag{16}$$

where, x_{ou} and x_{ov} are the separation distances up to the zero-cross of $C_{uu}(\Delta x)$ and $C_{vv}(\Delta x)$, respectively. In this case, $L_u/h=0.31$ and $L_v/h=0.075$ are obtained. This value of L_u/h is in good agreement with the previous values[22], and of course, it is much larger than L_v/h. If C_{uu} and C_{vv} can be approximated by an exponential function, then $C_{uu}(\Delta x)=\exp(-\Delta x/L_u)$ and $C_{vv}(\Delta x)=\exp(-\Delta x/L_v)$, which are shown by the broken lines in Fig. 8. Although the measured data can be roughly described by the exponential function, a large difference between the two appears when Δx is small, i. e. $\Delta x \leq 1$cm.

Since the eddies are convected with a velocity U_c, the peak of C_{uu} or C_{vv} appears at a time lag for any separation Δx, which is referred to the optimum delay τ_{opt}, as shown in Fig. 7. Fig. 9 shows $C_{uu}(\Delta x, \tau_{opt})$ and $C_{vv}(\Delta x, \tau_{opt})$ in this convected Eulerian frame. Indeed, the correlation of the v component decays rapidly and disappears. On the other hand, the correlation of u decays much more slowly, and does not disappear within the present measurement interval of $\Delta x/h \simeq 4$.

Incidentally, Blackwelder & Kovasznay (1972)[12] pointed out that $C_{uu}(\Delta x, \tau_{opt})$ and $C_{vv}(\Delta x, \tau_{opt})$ in the main region of the boundary layer could be well described by the sum of two exponential functions with decay rates differing by approximately one
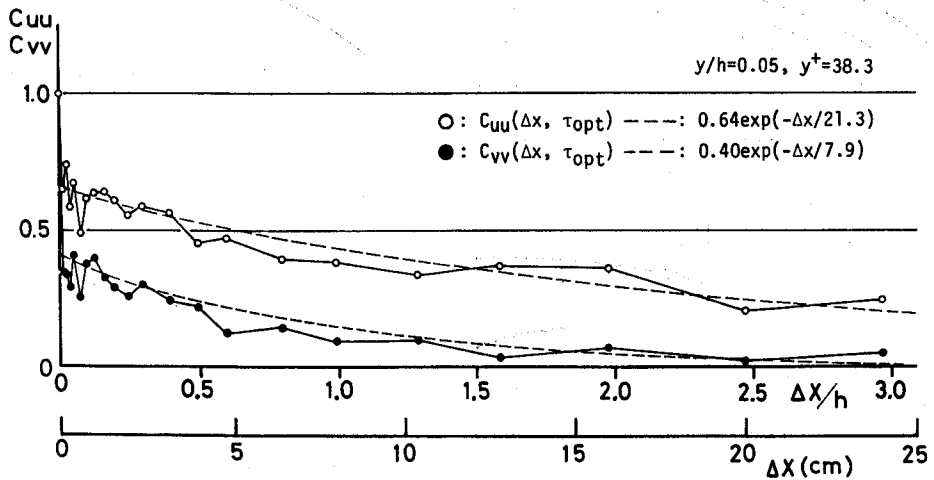

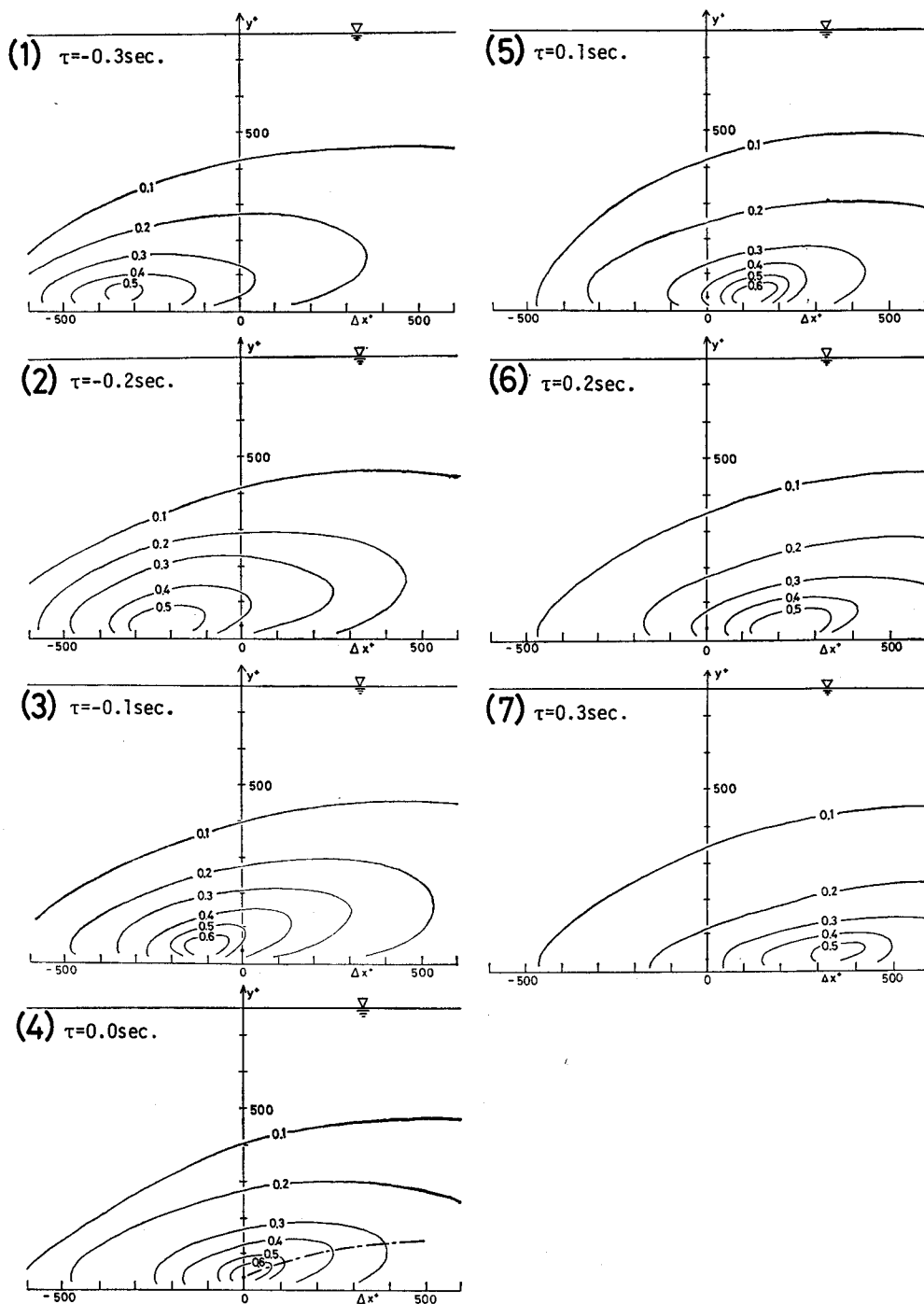Fig. 9. Space-time correlations of C_{uu} and C_{vv} with optimum delay.

Fig. 10.   Iso-correlation contours of C_{uu} when the time lag τ varies from -0.3 sec to 0.3 sec.

order of magnitude. The rapidly decaying curve is for the small eddies, while the slowly decaying curve is for the large eddies. However, the present results indicate only the slowly decaying exponential curve, as shown in Fig. 9. The $1/e$ folding separation for this large eddy structure is then $\Delta x = 2.6h$ and h for C_{uu} and C_{vv}, respectively. These values in the inner layer are the same order of those in the outer layer obtained by Blackwelder & Kovasznay, although the former is smaller than the latter.

Hence, it is considered that the small eddy structure has been filtered out in the present data of the correlations due to the setting of the spanwise separation $\Delta z = 2$mm when Δx is small. Indeed, this separation of Δz is comparatively large, since $\Delta z^+ \equiv \Delta z U_*/\nu = 19$ corresponds to $1/5$ of the spacing $\lambda^+ = 100$ between the low-speed streaks[22]. Therefore, the values near the origin in Figs. 8 and 9 are unreliable for discussing the fine structure of turbulence. However, this is of little concern for the present purposes.

Next, Fig. 10 shows the variation of the iso-correlation curves of C_{uu}, while the
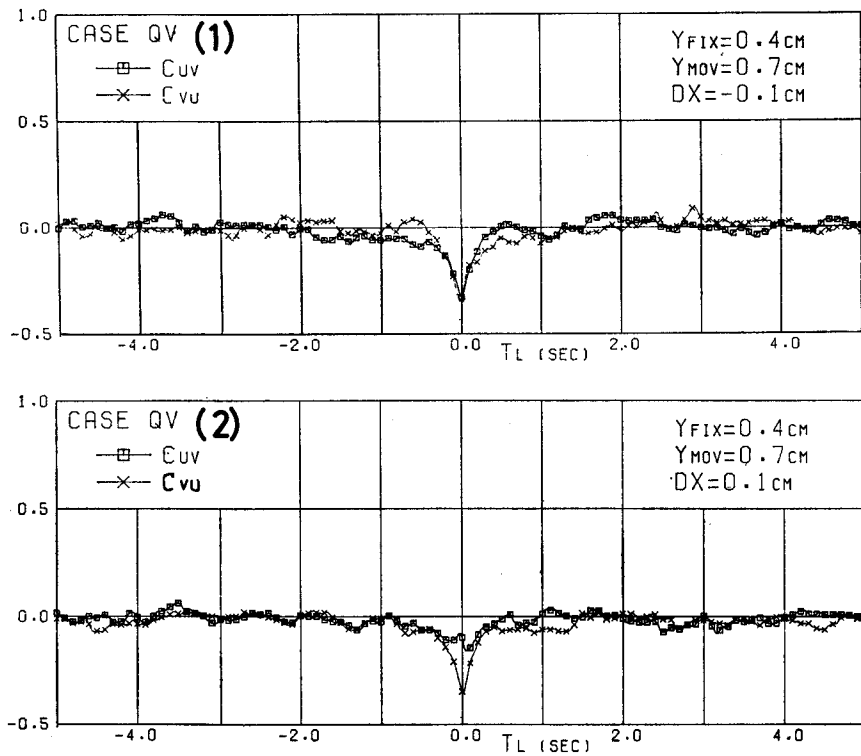

Fig. 11. An example of space-time cross correlations of u and v, C_{uv} and C_{vu}.

time lag τ varies from -0.3 sec to 0.3 sec. The large eddy structure is convected downstream without any remarkable deformation during this time. This convection velocity U_c is 13.2cm/sec as judged from Fig. 7, and it is nearly equal to the mean velocity $U=13.9$cm/sec at $y_0/h=0.05$. From Fig. 10(4), it is noticeable that the maximum correlation line fairly inclines downstream. This inclination angle toward the wall is 15-20 degrees near the center of the maximum iso-correlation, and it seems to become milder farther from the wall, which is in good agreement with the result of Blackwelder & Kovasznay (1972).

Lastly, Fig. 11 shows an example of C_{uv} and C_{vu}. C_{uv} must be nearly equal to C_{vu} when the separation distance between the two probes is small, i. e. $|C_{uv}(\tau=0)| \simeq |C_{vu}(\tau=0)| \simeq R = (0.3 \sim 0.4)$. However, there were some cases where $|C_{uv}| < |C_{vu}|$ appeared for the small positive values of Δx, as seen in Fig. 11(2). Although this cause is quite unknown at present, it may be that, as regards the v component, the resolution of the V-type probe is worse than that of the X-type probe when the shear stress is large. From Figs. 6 and 11, it is understood that the spatial and time scales of the Reynolds stress are much smaller than those of the u component.

4. 3 Eulerian time-correlations of bursting events by a new conditional sampling method

In order to investigate Eulerian time-correlations of bursting events measured at one position, we have firstly sorted the velocity signals u, v and the Reynolds-stress signals $-uv$ into the four quadrants of the u-v plane, as follows:

$$u_j(t) = u(t) \cdot I_j(t) \tag{17}$$

$$v_j(t) = v(t) \cdot I_j(t) \tag{18}$$

$$(-uv)_j(t) = -u(t)v(t) \cdot I_j(t) \tag{19}$$

where, $j=1$, 2, 3 and 4 (see $(5) \sim (8)$).

Next, by using the new conditional averaging method of (9) and (10), the Eulerian time-correlations $\langle \hat{u} \rangle_e(\tau)$, $\langle \hat{v} \rangle_e(\tau)$, $\langle -\hat{u}\hat{v} \rangle_e(\tau)$ and $\langle \hat{u} \rangle_s(\tau)$, $\langle \hat{v} \rangle_s(\tau)$, $\langle -\hat{u}\hat{v} \rangle_s(\tau)$ of each bursting event were obtained at $y_0^+ = y_1^+ = 38$, respectively. Figs. 12 and 13 show these results, in which the thirteen times ensemble averaging, i. e. the data size $N = 13 \times 10000$, was carried out in order to enhance the accuracy. The solid line in these figures indicates the total contributions from all events, that is, the conditional time-correlation of $\hat{u}$, $\hat{v}$ or $(-\hat{u}\hat{v})$, itself. Of course, $\langle \hat{u} \rangle_e \leq 0$, $\langle \hat{v} \rangle_e \geq 0$ and $\langle -\hat{u}\hat{v} \rangle_e \geq R$ during the ejection-phase (Fig. 12), in which the ejection motion is detected at $y_0^+ = 38$, while $\langle \hat{u} \rangle_s \geq 0$, $\langle \hat{v} \rangle_s \leq 0$ and $\langle -\hat{u}\hat{v} \rangle_s \geq R$ during the sweep-phase (Fig. 13). Obviously, the ejections are stronger than the sweeps, which is in good agreement with the previous results[2],[3] that $RS_2 > RS_4$ in Fig. 5. Also, the peak
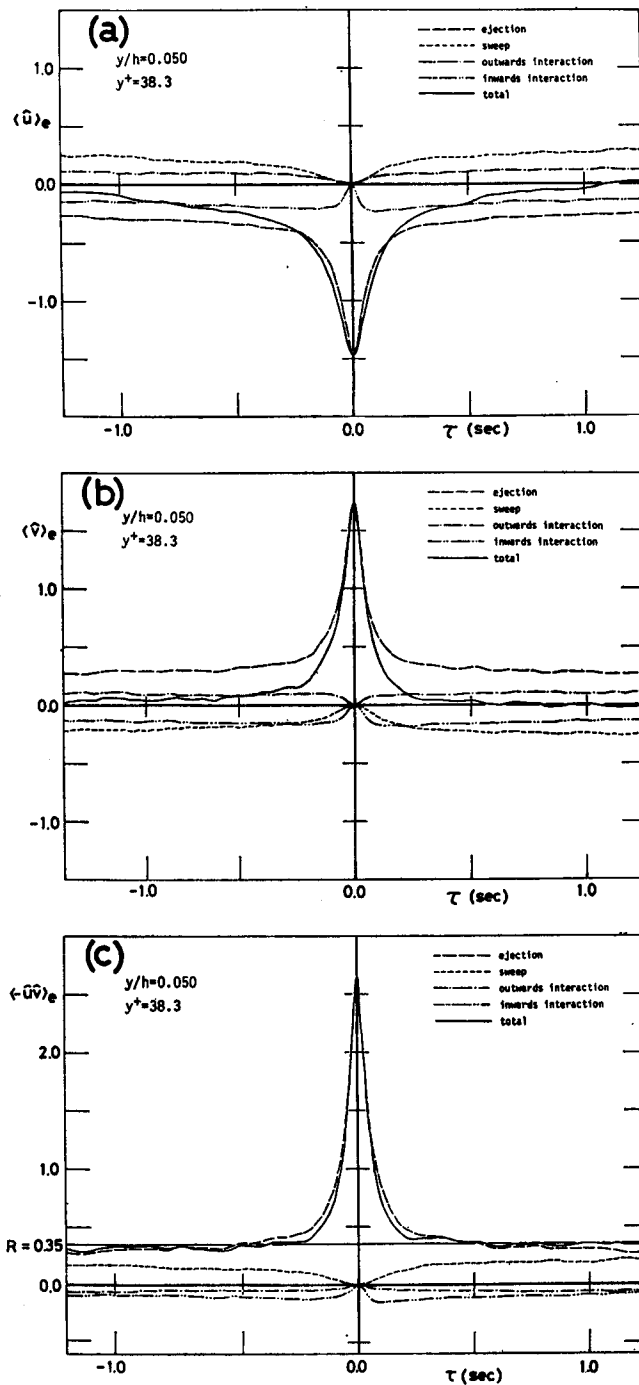
Fig. 12. Conditionally averaged time-correlations of u, v and $-uv$ when the ejection event is detected at $y^+ = 38$.
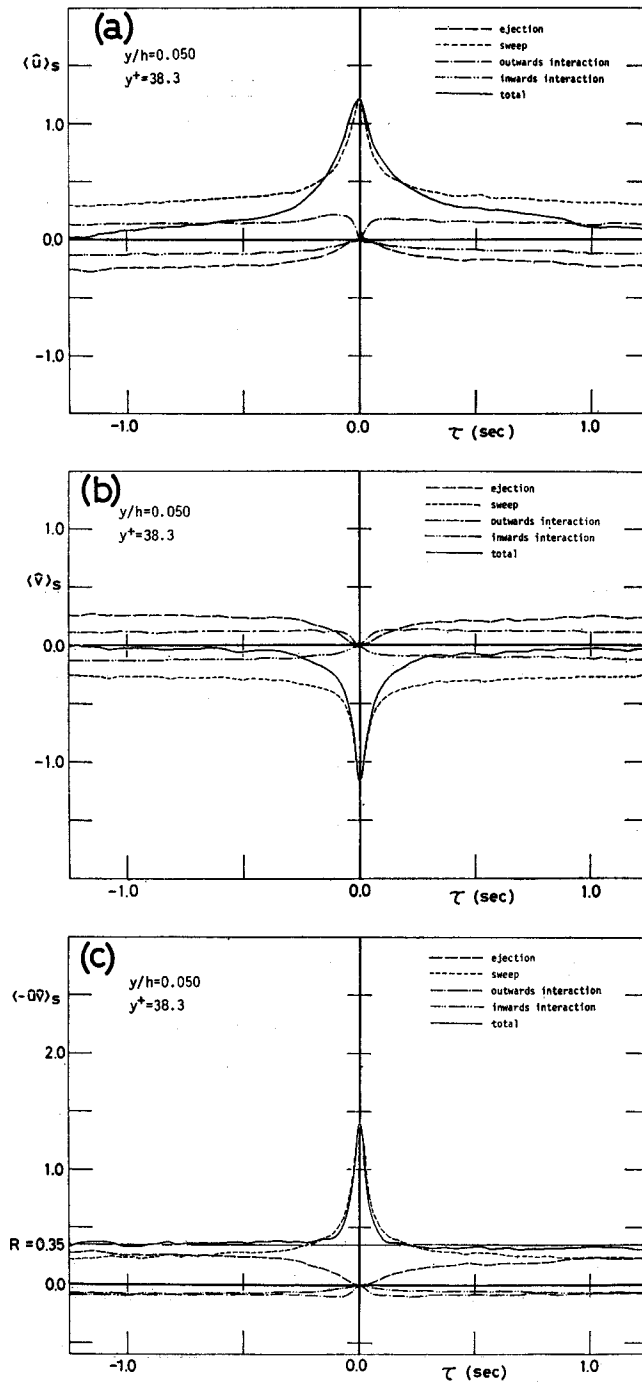
Fig. 13. Conditionally averaged time-correlations of u, v and $-uv$ when the sweep event is detected at $y^+ = 38$.

values of $\langle \hat{u} \rangle$, $\langle \hat{v} \rangle$ and $\langle -\hat{u}\hat{v} \rangle$ are comparable with the previous results which were obtained from the different detecting method with a threshold level (cf. 2. 2) by Lu & Willmarth (1973)[18] and Nakagawa & Nezu (1978)[4].

Since the conditional averages are asymmetric in regard to $\tau = 0$, the time scale $\mathscr{T}$ of the ejections and sweeps is defined separately as $\tau < 0$ and $\tau > 0$, in a way similar to (15) and (16), as follows:

$$\mathscr{T}_{\langle u \rangle_e -} = \int_{\tau -}^{0} \frac{\langle u \rangle_e(\tau)}{\langle u \rangle_e(0)} d\tau, \quad \mathscr{T}_{\langle u \rangle_e +} = \int_{0}^{\tau +} \frac{\langle u \rangle_e(\tau)}{\langle u \rangle_e(0)} d\tau \qquad (20)$$

where, $\tau -$ and $\tau +$ are the time lag up to the zero-cross of $\langle \hat{u} \rangle_e(\tau)$ for $\tau < 0$ and $\tau > 0$, respectively. The time scales of $\langle \hat{v} \rangle_e$, $\langle \hat{u} \rangle_s$ and $\langle \hat{v} \rangle_s$ are also defined in the same manner as (20). The time scales of the conditionally averaged Reynolds stress $\langle -\hat{u}\hat{v} \rangle_e$ and $\langle -\hat{u}\hat{v} \rangle_s$ are defined as follows:

$$\mathscr{T}_{\langle -uv \rangle -} = \int_{\tau -}^{0} \frac{\langle -\hat{u}\hat{v} \rangle(\tau) - R}{\langle -\hat{u}\hat{v} \rangle(0) - R} d\tau, \quad \mathscr{T}_{\langle -uv \rangle +} = \int_{0}^{\tau +} \frac{\langle -\hat{u}\hat{v} \rangle(\tau) - R}{\langle -\hat{u}\hat{v} \rangle(0) - R} d\tau \qquad (21)$$

The time scales evaluated from the above equations are described in Table 2. It is obvious that the time scale of the velocity component $\langle u \rangle$ is largest, while the time scale of the Reynolds stress $\langle -uv \rangle$ is smallest, for both ejections and sweeps. This confirms again that the instantaneous Reynolds stress shows an intermittent or pulse-like behaviour, which has been already revealed both theoretically and experimentally by the authors[3]~[5]. Also, it is suggested that the momentum transfer in the vertical direction (y) may be done in a short time, since $\mathscr{T}_{\langle v \rangle} < \mathscr{T}_{\langle u \rangle}$. From Figs. 12, 13 and Table 2, it can be generally concluded that the ejection motion occurs more violently and shortly than does the sweep motion, which coincides well with the previous visual observations[1],[2].

Next, as for the u and v components, $\mathscr{T}_- > \mathscr{T}_+$ during the ejection-phase, while $\mathscr{T}_- < \mathscr{T}_+$ during the sweep-phase. This suggests strongly that the ejection motion occurs

Table 2. Time scales $\mathscr{T}$ of the ejection and sweep motions.

	$\mathscr{T}_- U_{max}/h$ ($\tau < 0$)	$\mathscr{T}_+ U_{max}/h$ ($\tau > 0$)	$\mathscr{T} U_{max}/h$ $\mathscr{T} \equiv (\mathscr{T}_- + \mathscr{T}_+)/2$
Ejections			
$\langle \hat{u} \rangle_e$	0. 67	0. 50	0. 59
$\langle \hat{v} \rangle_e$	0. 34	0. 22	0. 28
$\langle -\hat{u}\hat{v} \rangle_e$	0. 16	0. 18	0. 17
Sweeps			
$\langle \hat{u} \rangle_s$	0. 68	0. 85	0. 77
$\langle \hat{v} \rangle_s$	0. 28	0. 36	0. 32
$\langle -\hat{u}\hat{v} \rangle_s$	0. 14	0. 10	0. 12

slowly and then decays rapidly, while the sweep motion occurs rapidly and then decays slowly, which is again consistent with visual observation[2]. Consequently, in the Eulerian observation the transition from the ejection to sweep motions occurs more rapidly than does the transition from the sweep to ejection motions. This coincides well with the results obtained from the other conditional analysis, i. e. VITA-method, by Blackwelder & Kaplan (1976)[20] and also the renewal model by Nakagawa & Nezu (1978)[4]. On the other hand, as for the Reynolds-stress signals, the opposite tendency appears, although the difference between $\mathscr{T}_-$ and $\mathscr{T}_+$ is small in both ejections and sweeps. This may be due to a greater contribution of the sweep event to $\mathscr{T}_+$ of the ejection-phase (see Fig. 12 (c)), and also of the ejection event to $\mathscr{T}_-$ of the sweep-phase (see Fig. 13(c)), since the transition from the ejection to sweep motions occurs more rapidly.

Finally, the results of the present quadrant analysis are consistent with those obtained from the pattern-recognition technique by Wallace et al. (1977)[21]. However, the detailed comparison cannot be done, since the former has the real time axis τ, while the latter has the time axis normalized by each bursting period. It should be noticed that the inward-interaction event coexists up to near the origin $\tau=0$ during the ejection-phase (see Fig. 12), while the outward-interaction event coexists during the sweep-phase (see Fig. 13). This has been already inferred theoretically by the authors[3].

4. 4 Space-time structure of bursting motions by the present conditional analysis

If the signals $\hat{u}_{mov}$ and $\hat{v}_{mov}$ of the movable probe are substituted for q in (9) or (10), we can obtain the space-time structures $<\hat{u}>(\tau)$ and $<\hat{v}>(\tau)$ when the ejection motion or the sweep motion occurs at the fixed probe ($y^+_{fix}=38$). Figs. 14-16 show several examples of such data described by the X-Y plotter.

Fig. 14 shows some results obtained in the wall region, i. e. at $y^+_{mov}=y^+_{fix}=38$, in which the separation Δx varied from $-0.5h$ up to $4h$. The smaller the separation $|\Delta x|$ is, the larger the peaks of $<u>$ and $<v>$ patterns become. Obviously, the averaged patterns of recognized u and v are approximately 180° out of phase, and this agrees with the results by Wallace et al. (1977)[21]. Of course, these patterns for the very small separation (Fig. 14 (3), (4)) should coincide well with the patterns for $\Delta x=0$, as shown in Figs. 12 and 13.

The peaks of $<u>$ and $<v>$ decrease gradually and also become flatter, with an increase of Δx. However, the $<v>$ pattern for the larger separation (see Fig. 14 (8)) may show only the ripple scattering, since the v-component decayed more rapidly. Also, its probe resolution was worse than the u-component, as mentioned previously. It is seen most clearly in Fig. 14(7) that the cyclic pattern of the ejection-sweep-ejection motions appears on an average, as observed visually[1],[4]. Furthermore, the transition from the ejection (e) to sweep (s) motions occurs more rapidly than the
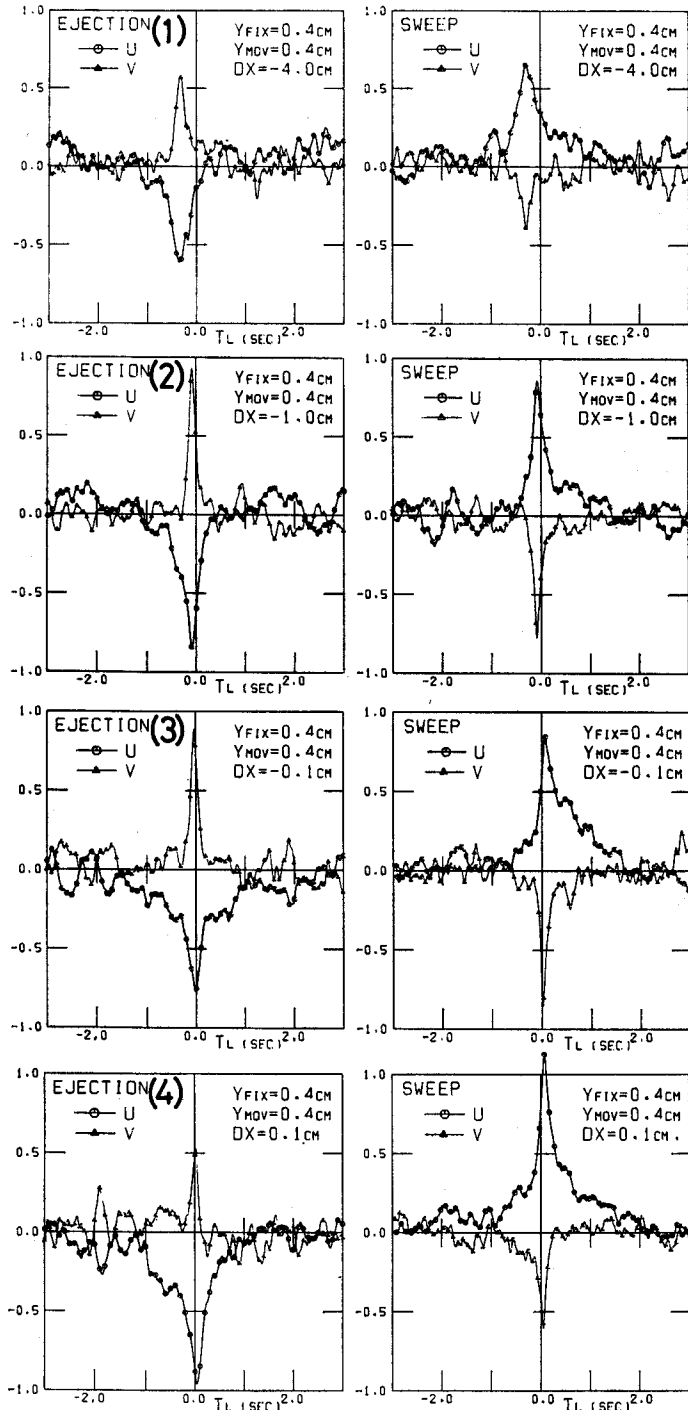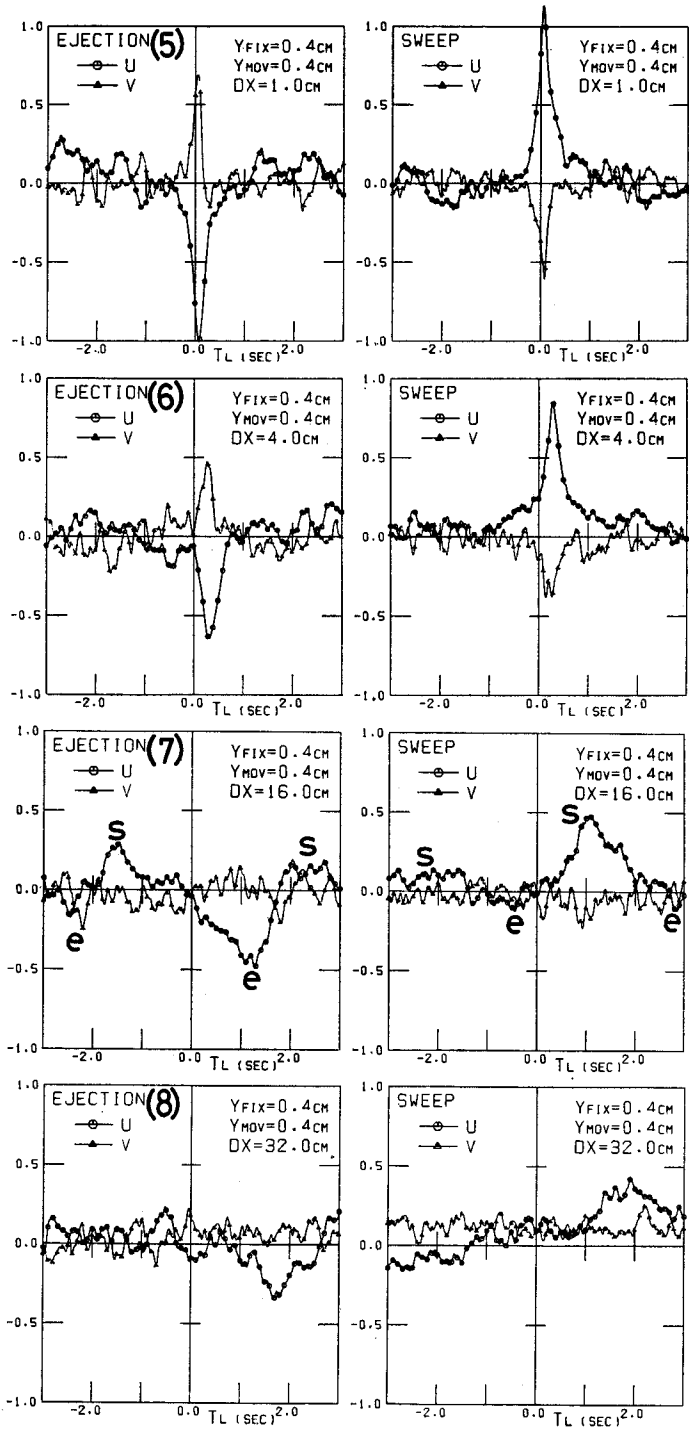
Fig. 14. Conditionally averaged space-time correlations $\langle \hat{u} \rangle (\tau)$ and $\langle \hat{v} \rangle (\tau)$ in the wall region (i. e. at $y^+ = 38$) when the ejection motion or the sweep motion occurs at the fixed probe ($y^+_{fix} = 38$).
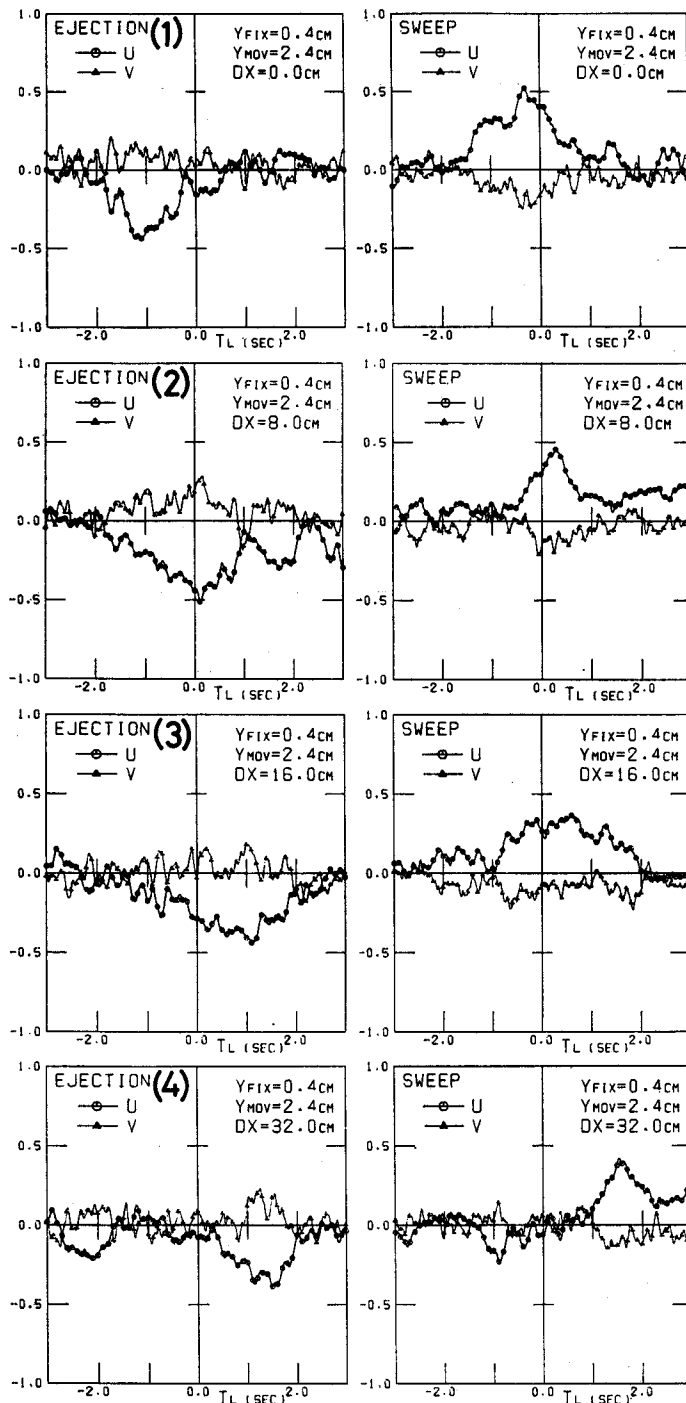
Fig. 15. Conditionally averaged space-time correlations $\langle \hat{u} \rangle (\tau)$ and $\langle \hat{v} \rangle (\tau)$ in the equilibrium region (i. e. at $y/h = 0.3$).
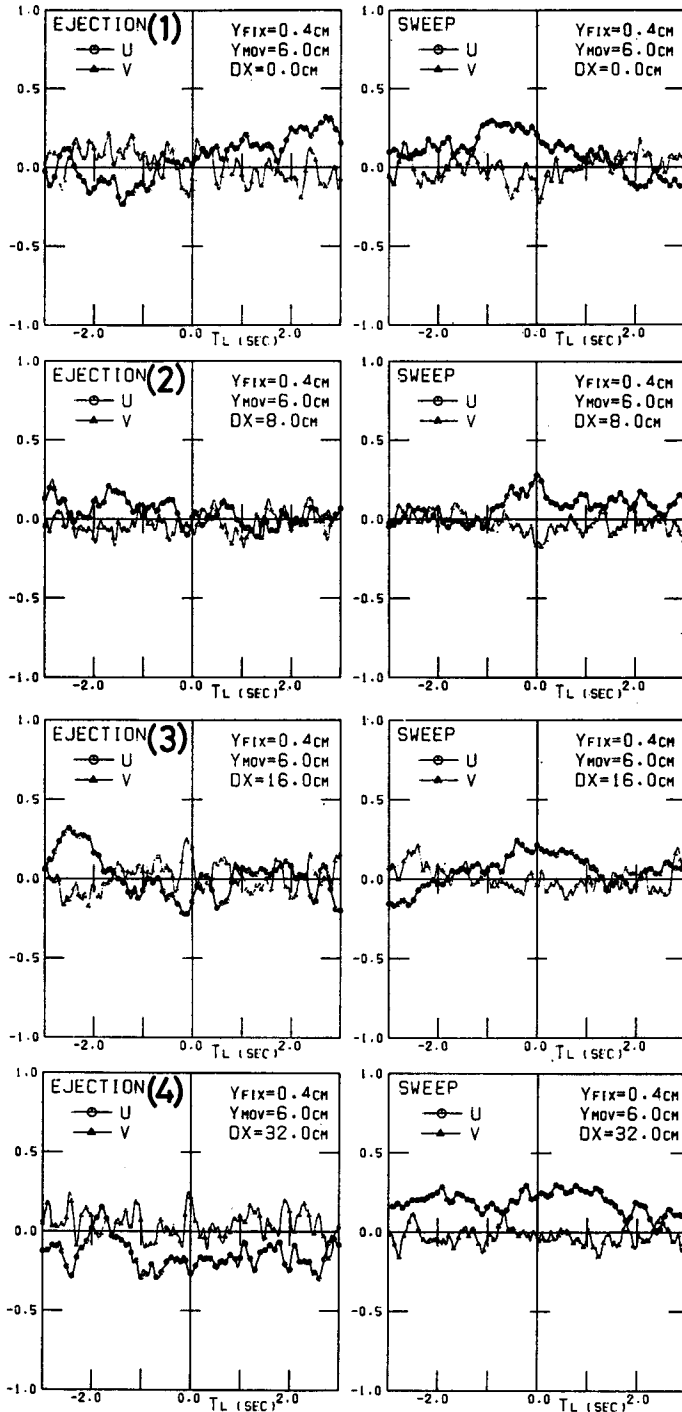
Fig. 16. Conditionally averaged space-time correlations $\langle \hat{u} \rangle (\tau)$ and $\langle \hat{v} \rangle (\tau)$ in the free-surface region (i.e. at $y/h = 0.75$).

reverse transition (s)→(e), which is considered to be one of the most essential characteristics of the bursting phenomenon.

Figs. 15 and 16 show some typical results in the equilibrium and the free-surface regions, respectively[22]. Although the general properties of the $\langle u \rangle$ and $\langle v \rangle$ patterns are the nearly same as Fig. 14, their peaks appear at the negative time lag when $\varDelta x=0$. This means that the phase of bursting motions in the region far from the wall goes ahead of that at the detecting position $y^+_{fix}=38$ near the wall. Another striking feature is that the bursting motion occurring in the wall region extends up to the free-surface region (see Fig. 16, where $y_{mov}/h=0.74$), although the $\langle v \rangle$ pattern may have comparatively large errors. Also, some examples that the states of $\langle u \rangle < 0$ (ejection-phase) and $\langle u \rangle \gg 0$ (sweep-phase) continue stably and longer than the bursting period[4], have been obtained for the larger separation $\varDelta x \geq 3h$ in the free-surface region, as seen in Fig. 16 (4). This suggests that there may exist an interrelation between the bursting motion and the stable high- and low-speed streaks or the boils observed on the free-surface of a river[25].

Next, Fig. 17 shows the space structures of $\langle \hat{u} \rangle (\varDelta x)$ and $\langle \hat{v} \rangle (\varDelta x)$ of the ejection and sweep motions at $y^+=38$, for $\tau=0$ by the solid line and $\tau=\tau_{opt}$ by the broken line at which both $\langle \hat{u} \rangle (\varDelta x)$ and $\langle \hat{v} \rangle (\varDelta x)$ attain the peaks. The results in the case of $\varDelta x < 0$ were also the nearly same as Fig. 17. These characteristics are roughly similar to those of the conventional long-time averaging structures in Figs. 8 and 9. It is easily understood that the u-component keeps its coherent structure over a longer distance than the v-component does. The same is also true for the sweeps than the ejections. In order to evaluate quantitatively the spatial scales $\mathscr{L}$ of the ejections and sweeps for $\tau=0$, we define the following in the same manner as (20):

$$\mathscr{L}_{\langle u \rangle_e -}=\int_{\varDelta x-}^{0} \frac{\langle u \rangle_e (\varDelta x)}{\langle u \rangle_e (0)} d(\varDelta x), \quad \mathscr{L}_{\langle u \rangle_e +}=\int_{0}^{\varDelta x+} \frac{\langle u \rangle_e (\varDelta x)}{\langle u \rangle_e (0)} d(\varDelta x), \text{ etc.} \quad (22)$$

The results evaluated from (22) are described in Table 3, separately for $\varDelta x < 0$ and $\varDelta x > 0$. If the bursting motions are convected downstream in the frozen-turbulence manner, we can obtain

$$\mathscr{L}_{\langle u \rangle_e -}=U_{c,\langle u \rangle_e} \times \mathscr{T}_{\langle u \rangle_e +}, \quad \mathscr{L}_{\langle u \rangle_e +}=U_{c,\langle u \rangle_e} \times \mathscr{T}_{\langle u \rangle_e -}, \text{ etc.} \quad (23)$$

Since the time scales $\mathscr{T}$ have been given in Table 2, and also the convection velocity U_c of each bursting motion is easily obtained as described in the next section, the spatial scales of (23) can be evaluated and are indicated in the parenthesis of Table 3. The data from (22) are fairly smaller than the data from (23), probably due to the inaccuracy of the profiles near the origin in Fig. 17, which were caused by the spanwise separation $\varDelta z$, as pointed out previously. However, the characteristics of the two are similar in the following respects.
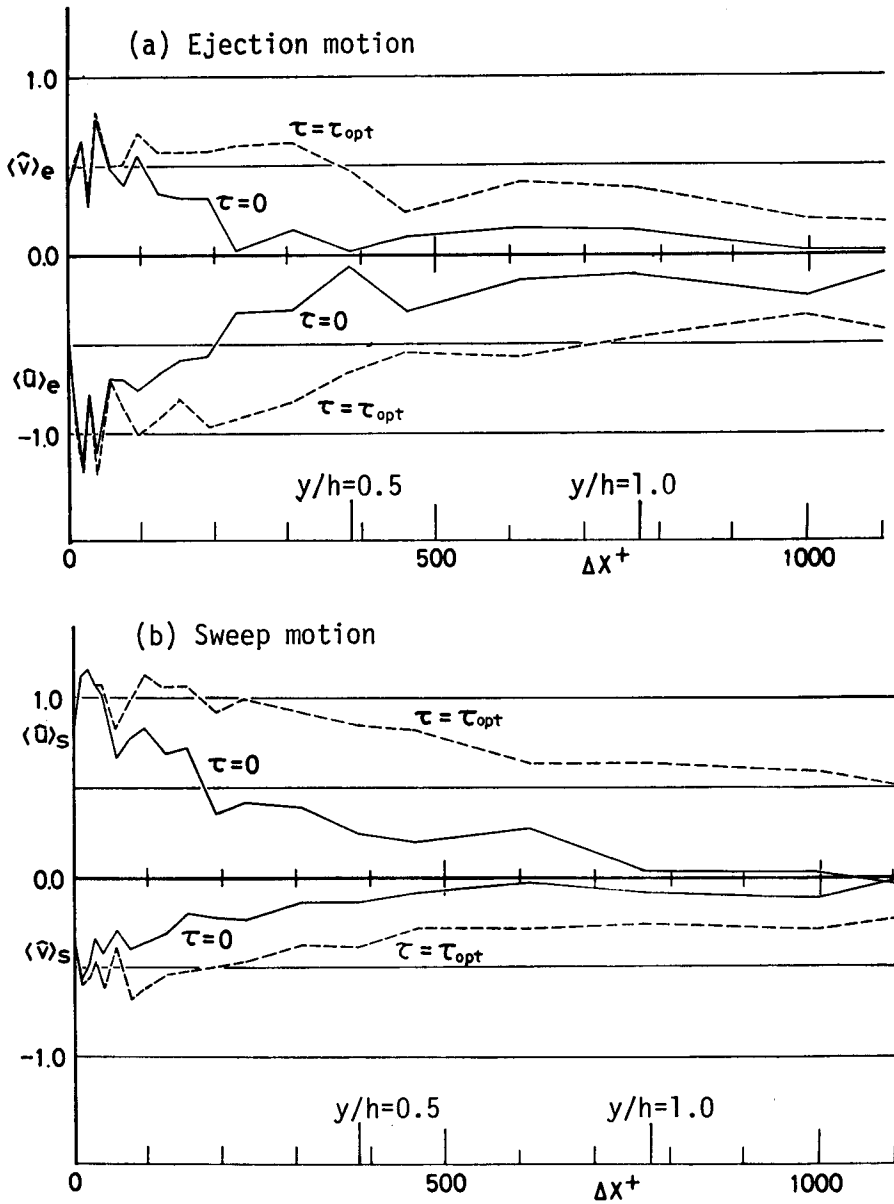
Fig. 17.   Space structures of $\langle \hat{u} \rangle(\Delta x)$ and $\langle \hat{v} \rangle(\Delta x)$ of the ejection and sweep motions observed at $y^+ = 38$.

Table 3. Spatial scales $\mathscr{L}$ of the ejection and sweep motions.

	$\mathscr{L}_-/h$ ($\Delta x<0$)	$\mathscr{L}_+/h$ ($\Delta x>0$)	Mean value $\mathscr{L}=(\mathscr{L}_-+\mathscr{L}_+)/2$
Ejections			
$\langle u\rangle_e$	0.24 (0.28)	0.28 (0.38)	0.26 (0.33)
$\langle v\rangle_e$	0.09 (0.13)	0.13 (0.20)	0.11 (0.16)
Sweeps			
$\langle u\rangle_s$	0.41 (0.59)	0.33 (0.47)	0.37 (0.53)
$\langle v\rangle_s$	0.17 (0.24)	0.13 (0.18)	0.15 (0.21)
Mean eddy			
L_u/h			0.31
L_v/h			0.08

The value in the parenthesis is equal to (the time-scale) × (the convection velocity), i. e. $\mathscr{T} \times U_c$.

(i) The spatial scale of u is larger than that of v.

(ii) The spatial scale of the sweeps is larger than that of the ejections.

(iii) The spatial scale of the ejections extends more widely downstream rather than upstream, i. e. $\mathscr{L}_-<\mathscr{L}_+$, and vice versa for the sweeps.

(iv) The spatial scales $\mathscr{L}$ of the bursting motions coincide roughly with the mean eddy scales L_u and L_v given by (15) and (16).

These characteristics infer that the bursting motion is a kind of large eddy structure and it is convected very coherently, i. e. with a frozen-turbulence-like pattern.

Futhermore, Fig. 18 shows the spatial patterns of $\langle u\rangle_e$ and $\langle u\rangle_s$ for $\tau=0$ at each different position y_{mov}. Here, the following characteristic-scale $\mathscr{L}$ is defined:

$$\mathscr{L}_{\langle u\rangle_e}(y) =\frac{1}{2}\int_{\Delta x-}^{\Delta x+}\frac{\langle u\rangle_e(\Delta x, y)}{\langle u\rangle_e(\Delta x=0,\ y_{fix})}d(\Delta x), \quad \text{etc.} \tag{24}$$

where, Δx_- and Δx_+ are the zero-crossing positions, between which there exists a peak of $\langle u\rangle$. Of course, $\mathscr{L}(y_{fix})=(\mathscr{L}_-+\mathscr{L}_+)/2$ in Table 3. $\mathscr{L}$ may be favorably called '*the influence scale of the bursting motion*', due to its definition of (24). Fig. 19 shows the influence scale $\mathscr{L}$ of the bursting motions, in which the data at $y/h=0.74$ could not be obtained because Δx_+ was out of the measurement range, i. e. $\Delta x_+>4h$. The relationship that $\mathscr{L}_{\langle u\rangle_s}>\mathscr{L}_{\langle u\rangle_e}>\mathscr{L}_{\langle v\rangle_s}>\mathscr{L}_{\langle v\rangle_e}$ is seen again. A noticeable tendency is that the influence scale increases with an increase of y^+ in the wall region ($y^+\leq100$), while it decreases with y^+ in the equilibrium region or the outer layer. This suggests that the bursting motions occurring near the buffer layer develop up to the
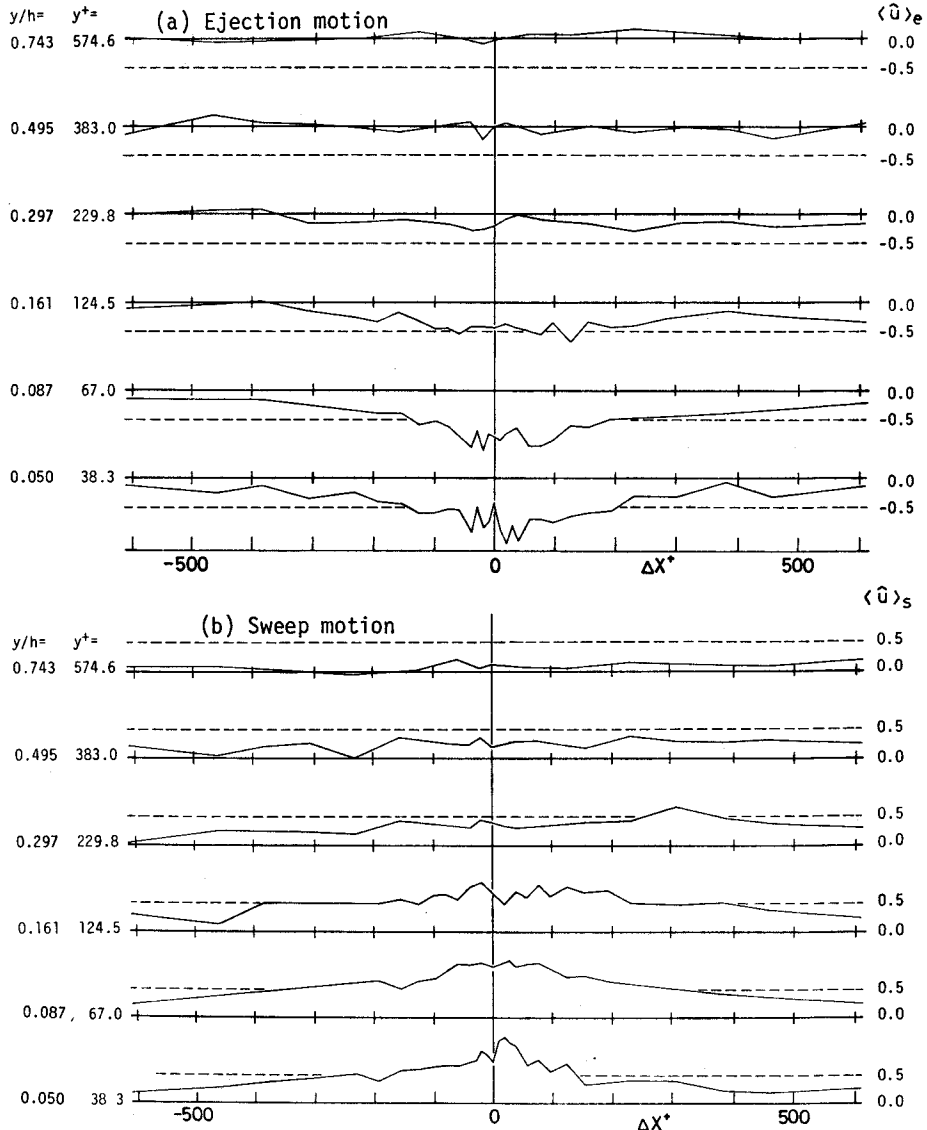
Fig. 18.   Spatial patterns of $\langle u \rangle_e$ and $\langle u \rangle_s$ for $\tau = 0$ obtained at each
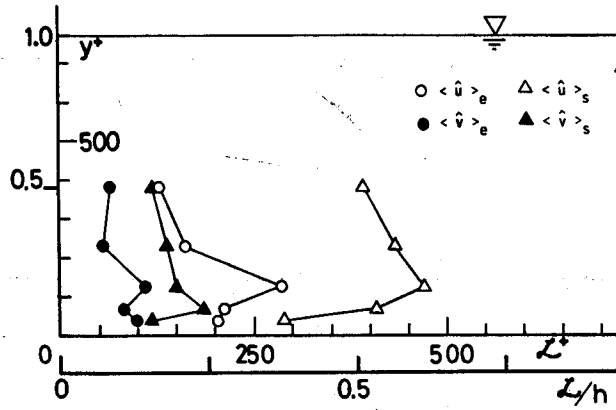   different position y_{mov}.

Fig. 19. Influence scale of the bursting motions.

edge of the wall region and then decay gradually in the outer layer, which is nearly consistent with visual observation by Offen & Kline (1975)[13].

4. 5 Convection process of the bursting motions

Figs. 20 and 21 show the spatial iso-patterns of the $\langle \hat{u} \rangle$ and $\langle \hat{v} \rangle$ components
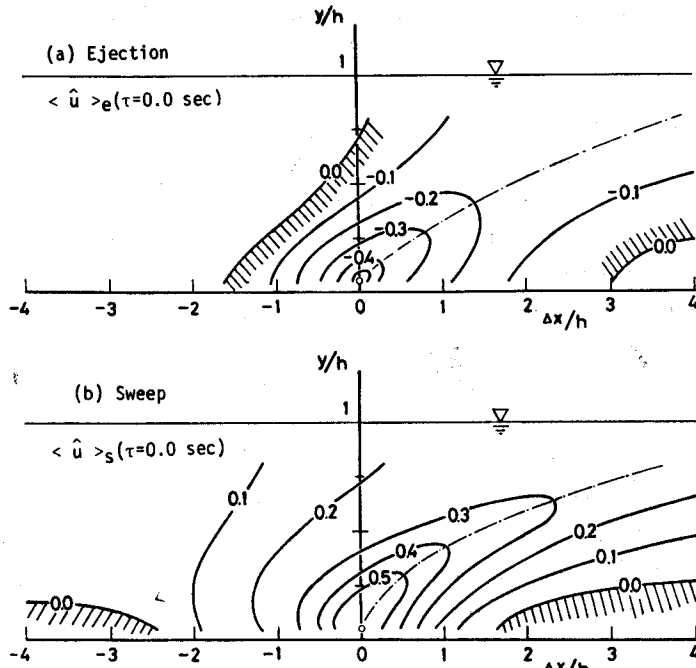

Fig. 20. Spatial iso-patterns of $\langle \hat{u} \rangle$ at the instant when the ejection and sweep motions occur at $y^+ = 38$.
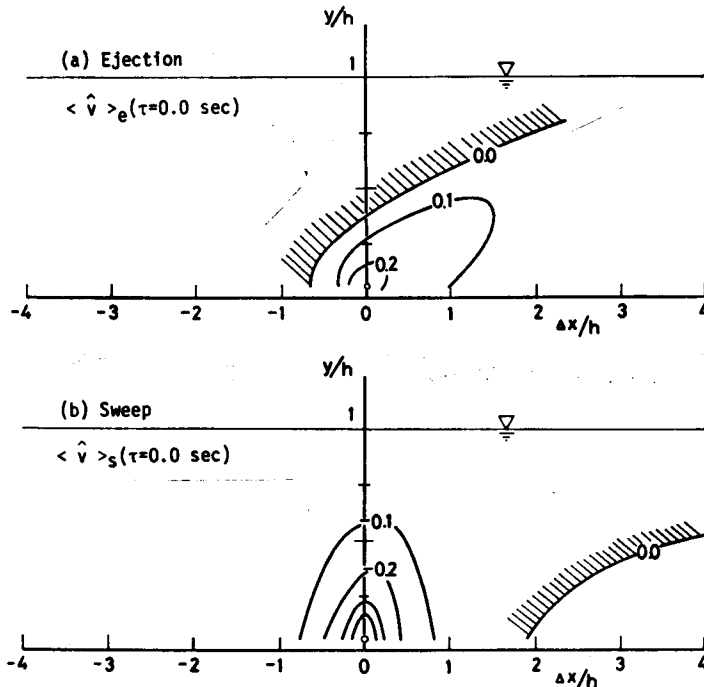
Fig. 21. Spatial iso-patterns of $\langle \hat{v} \rangle$ at the instant when the ejection
and sweep motions occur at $y^+ = 38$.

respectively, at the instant when the ejection or sweep motions occur at $y^+ = 38$. To discriminate easily, the negative regions of $\langle \hat{u} \rangle$ and $\langle \hat{v} \rangle$ are hatched. Evidently, the spatial pattern of $\langle \hat{u} \rangle$ is fairly inclined downstream, similar to the large eddy in Fig. 10. According to the detailed examination in the region $|\Delta x| \leq h$ where the measurement has been densely performed as shown in Fig. 2(b), the inclination angles of the iso-lines of $\langle \hat{u} \rangle_e$ and $\langle \hat{u} \rangle_s$ toward the wall are both about $20° \sim 25°$ near the detecting probe. Then, they become milder as they go farther from the wall, that is: about $10°$ near the middle flow depth. On the other hand, the iso-patterns of $\langle \hat{v} \rangle$ do not show any conspicuous inclination characteristic in the wall region at least, but $\langle \hat{v} \rangle$ has the strongest correlation in the vertical direction. Comparing the difference of these inclinations between the $\langle u \rangle$ and $\langle v \rangle$ patterns, the v-fluctuation involved in the ejection and sweep motions seems to decay more rapidly than does the u-fluctuation, since the former is apt to be more influenced by the velocity shear. Consequently, the scale of the $\langle v \rangle$ pattern may become smaller than that of the $\langle u \rangle$ pattern, as mentioned previously. By comparison between the ejection and sweep motions, the spatial-scale characteristics of the bursting motions given in the previous section are clearly understood again.
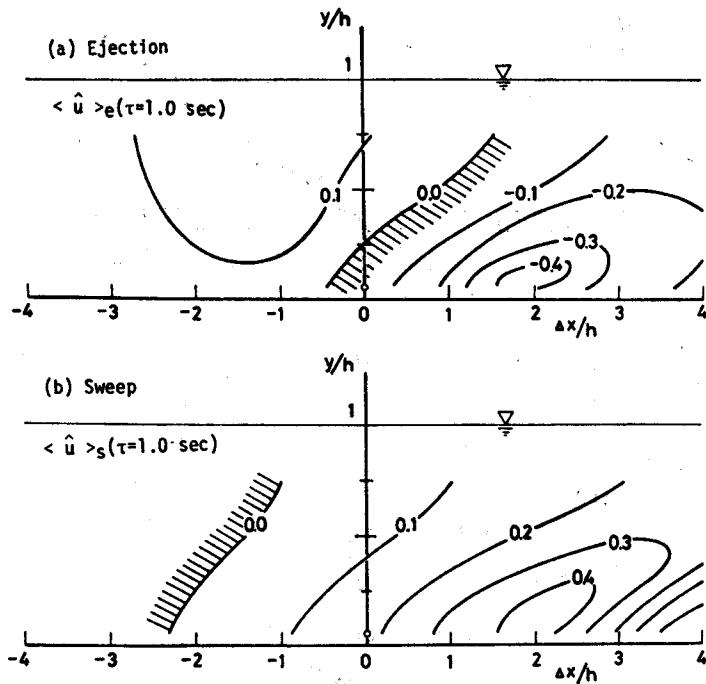
Fig. 22. Spatial iso-patterns of $\langle \hat{u} \rangle$ at the time when $\tau U_{max}/h = 2.6$
passed after the occurrence of the bursting motion at the
detecting probe.

Next, Fig. 22 shows the iso-patterns of $\langle \hat{u} \rangle$ at one second after the occurrence of the bursting motion at the detecting probe. This elapsing time $\tau U_{max}/h = 2.6$ corresponds to the bursting (passing-) period $T_B U_{max}/h = (1.5\text{-}3.0)$[4]. By comparison with Fig. 20, the most striking characteristic is that the $\langle u \rangle$ pattern of the bursting motions is surely convected downsteam without its remarkable deformation, namely in the frozen-turbulence-like manner. This is considered to be caused by the following: (1) The Lagrangian life-time T_l of the u-fluctuation involved in the bursting motions is much larger than the bursting period T_B. Since the bursting motion is a kind of the large coherent-eddies, $T_l U_{max}/h$ may be roughly larger than 10, as inferred from the result by Blackwelder & Kovasznay (1972)[12] (2) Its convection velocity in the vertical direction, which is comparable to v', is much smaller by one order of magnitude than the convection velocity U_c in the streamwise direction, that is, $v'/U_c \simeq 0.1$.

Lastly, Figs. 23 and 24 show the optimum delay time τ_{opt} of $\langle u \rangle$ and $\langle v \rangle$ against the separation Δx, respectively. Although the data in the region far from the wall scatter each other due to the flatter profile of $\langle \hat{u} \rangle(\tau)$ and $\langle \hat{v} \rangle(\tau)$, it is noticeable that the convection velocity of the sweep motion is a little larger than that of the
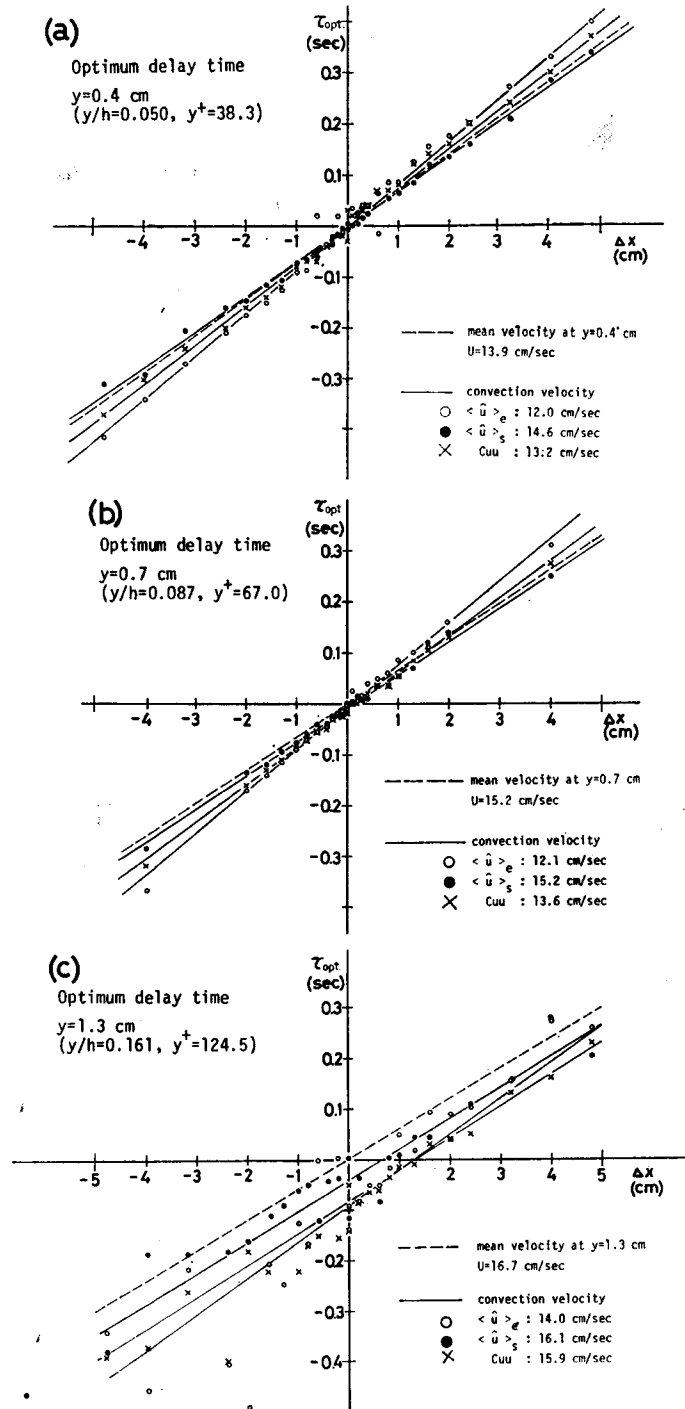
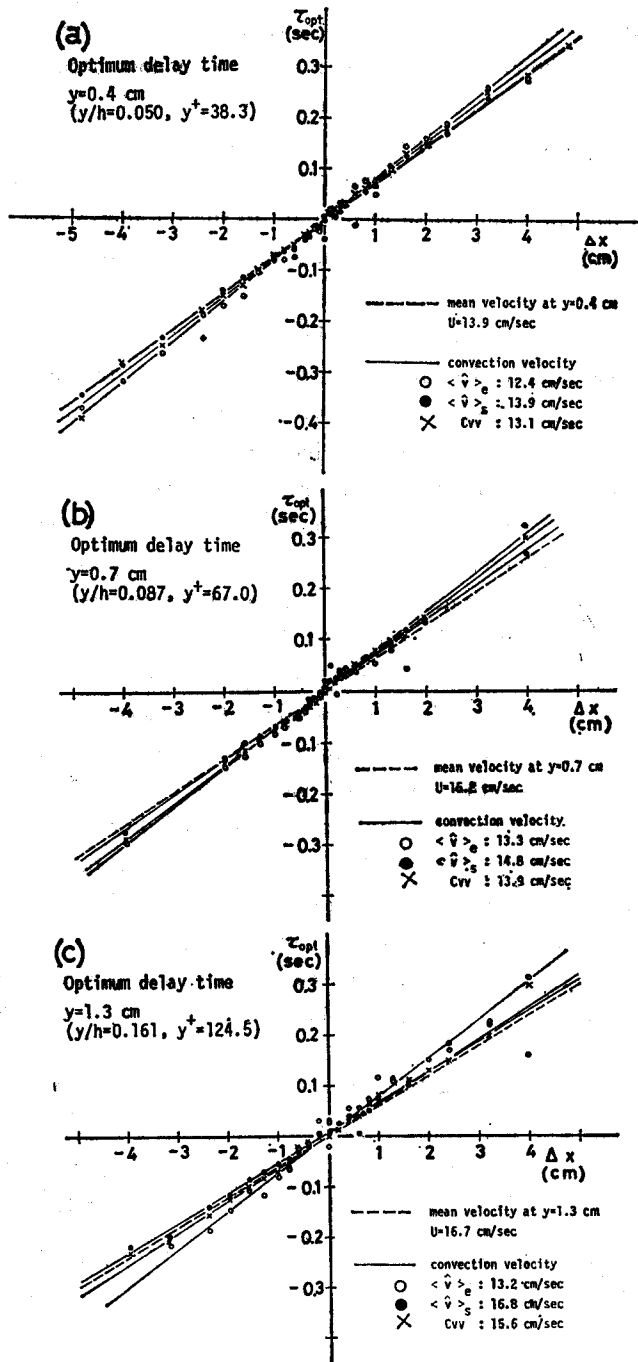Fig. 23. Optimum delay time τ_{opt} of $\langle u \rangle$ against the separation Δx.

Fig. 24. Optimum delay time τ_{opt} of $\langle v \rangle$ against the separation Δx.

ejection motion. The average of the two becomes nearly equal to the convection velocity of a large eddy observed by the conventional long-time average of 4.2. In particular, the convection velocity of the ejection motion becomes nearly equal to $U_{c,<u>_e}/U \simeq 0.8$, which agrees well with the result by Lu & Willmarth (1973)[18]. Another outstanding feature is that the phase of the $<u>$ pattern far from the wall goes ahead of that near the wall (compare Fig. 23, (a) with (c)), while the $<v>$ pattern has nearly the same phase at least up to the outside of the wall region (see Fig. 24). This explains again the inclination characteristics of the bursting motions.

4.6 Qualitative model of the bursting phenomenon

A phenomenological model to describe the space-time structures of the bursting phenomenon is proposed here on the basis of the above results, and its simplified model is shown in Fig. 25. It can be judged from the present study and other visual studies that there surely exist a high-speed region and a low-speed region alternately in an open-channel flow, although the velocity difference between the two regions may be not so large. A high-speed region probably moves toward the wall with a small angle and comes into a low-speed region, as seen in Fig. 22 (a). Consequently, an interface or a high-speed front is formed between the high- and low-speed regions (see Fig. 25), although its sharp line of demarcation does not exist. An interaction between the high- and low-speed fluids is considered to be a coherent structure with an ejection and sweep motions. A sweep motion shown by A in Fig. 26, which is described in the convected view with its coherent structure, appears remarkably at a place immediately upstream of the high/low interface and far from the wall. Then an ejection motion, shown by B in Fig. 26, occurs remarkably at a place immediately downstream from the interface. It is one of the most characteristic points that the transition from the high-speed region on the upstream side to the low-speed region on the downstream side occurs more rapidly than the opposite transition, as shown in Fig. 25. Of course, this high/low interface has a three-dimensional
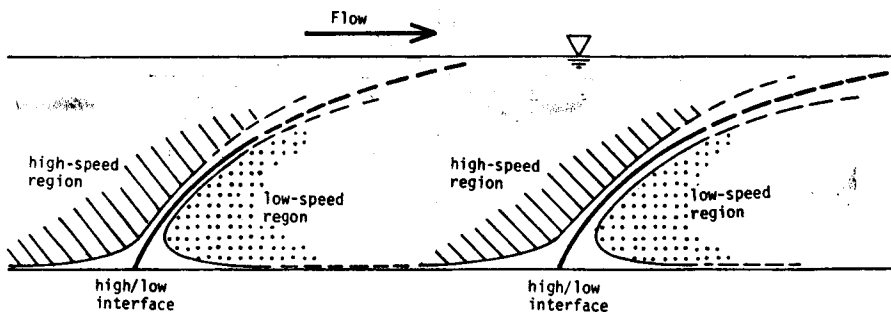

Fig. 25. A model of high- and low-speed regions in an open-channel flow.

structure, and moreover, it appears at random in space and time.   However, the
coherent structure near its interface is convected downstream with a longer life-time
at least than the bursting passing-period, namely in the frozen-turbulence-like manner.
Thus, in the Eulerian observation of its coherent structure, a cyclic variation (slow
deceleration of u)→(ejection motion)→(rapid transition to the sweep motion, i. e.
rapid acceleration of u)→(slow deceleration of u), can be recognized on an average.

We must consider the coherent bursting motions in three-dimensional aspects, although
the present experimental study dealt with the structure in the x-y plane.   According
to our earlier visual study (1977)[26] and many other visual studies, the spanwise
structure consists of high- and low-speed streaks whose spacing λ^+ is nearly equal to 100
in the wall region, but tends to increase gradually with y/h outside the wall region.
Fig. 26 shows a conceptual model of the bursting motions, in which the white and
the black arrows denote the high- and low-speed fluids, respectively, in regard to the
convected view with the coherent structure.   Since the high/low interface is fairly
inclined downstream toward the wall, a high-speed fluid (A) (i. e. a sweep motion),
penetrates toward the wall and plays a complicated interaction with a low-speed fluid
(B) (i. e. an ejection motion).   As a result of this interaction, (A) and (B) are
entangled with each other and combined into a spanwise outflow (C) and a high-
speed fluid (D) traveling along the interface which corresponds to an outward-
interaction motion (i. e. $u>0$ and $v>0$), due to a condition of continuity.   Of course,
this interaction itself corresponds to the mechanism of turbulence production.   (D)
develops in the outer layer and then its part (E) returns toward the wall.   Next, (E)
and an inflow (C′) from the neighbouring bursting motion are combined into a
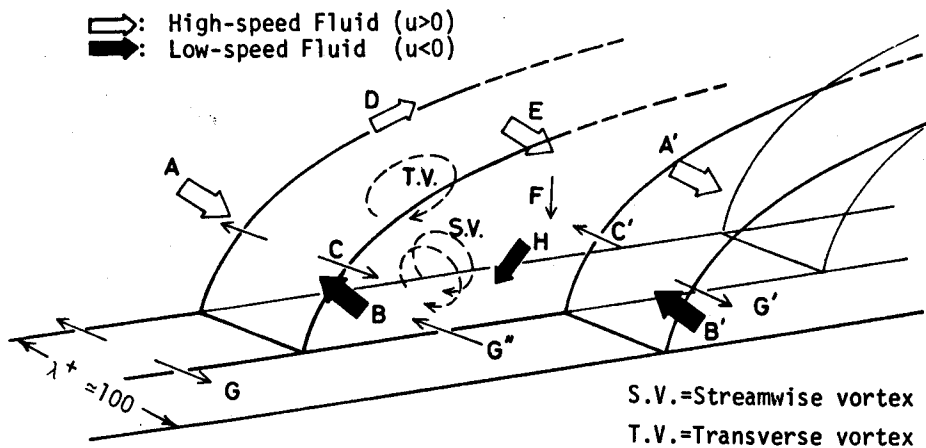downflow (F) and a new high-speed fluid (A′).   (F) comes into the low-speed

Fig. 26. A conceptual model of the bursting motions in an open-channel flow.

region and thus changes into a low-speed fluid (H), which may in part correspond to an inward-interaction motion (i. e. $u < 0$ and $v < 0$). As adding a spanwise inflow (G'') caused by a consequence of continuity of (C), the low-speed fluid (H) develops in the wall region due to a strong velocity shear stress, and then it is supplied to the ejection motion (B).

Consequently, such a sequence of these fluid motions forms and keeps a coherent structure over a longer convection-distance than several times of the flow depth. In this coherent structure, (D) and (E) form a transverse vortex near the high/low interface. It can be truly said that (D) and (E) are formed by a transverse vortex caused by a Helmholtz-type interaction between the high- and low-speed regions. An inflow and outflow, e. g. (G'') and (C), between the neighbouring spanwise structures also form a streamwise vortex, as shown in Fig. 26. Thus, the streamwise vortices appear more remarkably closer to the wall, while the transverse vortices appear more remarkably farther from the wall, which is in a good agreement with the visual observation by Praturi & Brodkey (1978)[14]. Indeed, a composite model of the streamwise and transverse vortices makes up a horseshoe vortex, which was first proposed by Theodorsen (1955)[27] and was then adopted as an origin of Black's model (1968)[8] and our Π-eddy model (1974)[28]. It was a little suggested from our visual observation[26] that such a horseshoe vortex might develop up to the outside of the wall region and then coalesce each other.

However, it has to be emphasized here that the present model of Fig. 26 has been proposed on a basis of the available fragmentary information of the conditionally ensemble-averaged velocity patterns $<u>$ and $<v>$. Thus, it is yet unknown whether a horseshoe vortex itself exists or not as a real-time coherent structure, as pointed out by Praturi & Brodkey (1978)[14].

From the above consideration, the present model can explain satisfactorily some of the most essential characteristics of the bursting motions obtained from the present anemometry study. Also, the present model corresponds very well with a model proposed by Praturi & Brodkey (1978)[14] who performed a notable stereoscopic visual study of coherent structures in a boundary layer flow.

5. Conclusions

The present study has investigated the structure of space-time correlations of bursting motions, such as ejections and sweeps in an open-channel flow, by a new conditional sampling analysis of the instantaneous velocity and Reynolds-stress signals measured simultaneously by two dual-sensor hot-film probes. One probe was fixed near the edge of the buffer layer and used as a detecting probe of the bursting motions. The other probe was moved in both the streamwise and vertical directions.

The main conclusions obtained from the above are as follows:

(1) The spatial and time scales of the streamwise turbulent velocity component are larger than those of the vertical velocity component.

(2) The spatial and time scales of the sweep motion are also larger than those of the ejection motion.

(3) The spatial scale of the ejection motion extends more widely downstream than upstream, and vice versa for the sweep motion.

(4) The bursting motion is a kind of large-scale eddy structure, and its coherent structure is fairly inclined downstream toward the wall. It is convected downstream with a longer life-time than the bursting passing-period, namely in the frozen-turbulence-like manner.

Next, a qualitative model has been proposed which attempted to explain the space-time structures of the bursting phenomenon, on the basis of the above fragmentary information and other visual information. The present model could explain satisfactorily some of the most essential characteristics of the bursting motions. However, a great part of the cause-and-effect relationship of bursting phenomenon or coherent vortex motions is yet unknown, even qualitatively. Above all, it is quite unknown why the high- and low-speed regions exist alternately in both the streamwise and spanwise directions in a turbulent shear flow. Hence, a more detailed experimental investigation of the bursting phenomenon by simultaneous anemometry and visual measurements is necessary.

References

1) Hinze, J. O.: *Turbulence* (2-nd ed.), McGraw-Hill, pp. 586-770, (1975).

2) Willmarth, W. W.: Structure of turbulence in boundary layers, Adv. Appl. Mech., vol. **15** pp. 159-254 (1975).

3) Nakagawa, H. and Nezu, I.: Prediction of the contributions to the Reynolds stress from the bursting events in open-channel flows, J. Fluid Mech., vol. **80**, pp. 99-128 (1977).

4) Nakagawa, H. and Nezu, I.: Bursting phenomenon near the wall in open-channel flows and its simple mathematical model, THIS MEMOIRS, Fac. Eng., Kyoto Univ., vol. **40**, pp. 213-240 (1978).

5) Nakagawa, H. and Nezu, I.: Structure of instantaneous Reynolds stress over a permeable open-channel with suction or injection, THIS MEMOIRS, Fac. Eng., Kyoto Univ., vol. **41**, pp. 240-267 (1979).

6) Einstein, H. A. and Li, H.: The viscous sublayer along a smooth boundary, Proc. of ASCE, EM-2, pp. 1-27 (1956).

7) Landahl, M. T.: A wave-guide model for turbulent shear flow, J. Fluid Mech., vol. **29**, pp. 441-459 (1967).

8) Black, T. J.: A new model of the shear stress mechanism in wall turbulence, AIAA 6-th Aero. Sci. Meeting, AIAA Paper No. 68-42 (1968).

9) Bark, F. H.: On the wave structure of the wall region of a turbulent boundary layer, J. Fluid Mech., vol. **70**, pp. 229-250 (1975).

10) Landahl, M. T.: Dynamics of boundary layer turbulence and the mechanism of drag reduc-

tion, Phys. of Fluids, vol. **20**, pp. S55-S63 (1977), also see 'Hydraulic problems solved by stochastic methods (ed. by Hjorth et al.), 2-nd Int. Symp. on Stochastic Hydraulics, pp. 1-22 (1977).

11) Laufer, J. and Narayanan, M. A. B.:   Mean period of the turbulent production mechanism in a boundary layer, Phys. of Fluids, vol. **14**, pp. 182-183 (1971).

12) Blackwelder, R. F. and Kovasznay, L. S. G.:   Time scales and correlations in a turbulent boundary layer, Phys. of Fluids, vol. **15**, pp. 1545-1554 (1972).

13) Offen, G. R. and Kline, S. J.:   A proposed model of the bursting process in turbulent boundary layers, J. Fluid Mech., vol. **70**, pp. 209-228 (1975).

14) Praturi, A. K. and Brodkey, R. S.:   A stereoscopic visual study of coherent structures in turbulent shear flow, J. Fluid Mech., vol. **89**, pp. 251-272 (1978).

15) Jackson, R. G.:   Sedimentological and fluid-dynamic implications of the turbulent bursting phenomenon in geophysical flows, J. Fluid Mech., vol. **77**, pp. 531-560 (1976).

16) Gupta, A. K., Laufer, J. and Kaplan, R. E.:   Spatial structure in the viscous sublayer, J. Fluid Mech., vol. **50**, pp. 493-512 (1971).

17) Kovasznay, L. S. G., Kibens, V. and Blackwelder, R. F.:   Large-scale motion in the intermittent region of a turbulent boundary layer, J. Fluid Mech., vol. **41**, pp. 283-325 (1970).

18) Lu, S. S. and Willmarth, W. W.:   Measurements of the structure of the Reynolds stress in a turbulent boundary layer, J. Fluid Mech., vol. **60**, pp. 481-511 (1973).

19) Brodkey, R. S., Wallace, J. M. and Eckelmann, H.:   Some properties of truncated turbulence signals in boundary shear flows, J. Fluid Mech., vol. **63**, pp. 209-224 (1974).

20) Blackwelder, R. F. and Kaplan, R. E.:   On the wall structure of the turbulent boundary layer, J. Fluid Mech., vol. **76**, pp. 89-112 (1976).

21) Wallace, J. M., Brodkey, R. S. and Eckelmann, H.:   Pattern-recognized structures in bounded turbulent shear flows, J. Fluid Mech., vol. **83**, pp. 673-693 (1977).

22) Nezu, I.:   *Turbulent structure in open-channel flows*, Ph. D thesis in Civil Engineering, Kyoto Univ. (1977).

23) Nezu, I.:   Turbulence intensities in open-channel flows, Proc. of JSCE, No. **261**, pp. 67-76 (1977) (in Japanese).

24) Favre, A. J.:Review on space-time correlations in turbulent fluids, Trans. of ASME, J. Appl. Mech., vol. **32**, pp. 241-257 (1965).

25) Kinoshita, R.:   An analysis of the movement of flood waters by aerial photography, Photographic Surveying, vol. **6**, pp. 1-17 (1967) (in Japanese).

26) Nakagawa, H. and Nezu, I.:   Visualization of wall turbulence in open-channel flow by hydrogen-bubble method, 5-th Symp. on Flow Visualization, ISAS, Univ. of Tokyo, No. **5**, pp. 47-50 (1977) (in Japanese).

27) Theodorsen, T.:   The structure of turbulence, 50 Jahre Grenzschichtforschung (ed. by Görtler & Tollmien) Frier. Vieweg & Sohn, pp. 55-62 (1955).

28) Nakagawa, H. and Nezu, I.:   On a new eddy model in turbulent shear flow, Proc. of JSCE, No. **231**, pp. 61-70 (1974).